CALCULATIONS OF ELECTRIC AND MAGNETIC PROPERTIES OF TRIANGULAR GRAPHENE FRAGMENTS USING DENSITY FUNCTIONAL THEORY: EFFECTS OF EDGE FUNCTIONALIZATION AND ELECTRIC FIELD

A Thesis Submitted to
the Graduate School of Engineering and Sciences of
İzmir Institute of Technology
in Partial Fulfillment of the Requirements for the Degree of

MASTER OF SCIENCE

in Physics

by
Fadıl İYİKANAT

July 2013
İZMİR

We approve the thesis of **Fadıl İYİKANAT**

Prof. Dr. Ramazan Tuğrul SENGER
Supervisor

Asst. Prof. Coşkun Kocabaş
Committee Member

Dr. A. Devrim Güçlü
Committee Member

11 July 2013

Prof. Dr. Nejat BULUT
Head of the Department of
Physics

Prof. Dr. Ramazan Tuğrul SENGER
Dean of the Graduate School of
Engineering and Sciences

ACKNOWLEDGMENTS

It is my pleasure to acknowledge and express my gratitude those who helped me along the way to completion of this thesis.

I wish to express my respect and sincere gratitude to my supervisor, Prof. Dr. R. Tuğrul Senger for his supervision, care and support during this thesis and also for giving me the opportunity to work in a very interesting field of research. He has always allowed me to pursue my own ideas. Without his encouragements, guidance and insight, I could not have finished this dissertation.

Besides my advisor, I would also like to thank the other members of my thesis defense committee Assist. Prof. Dr. Coşkun Kocabaş and Dr. Devrim Güçlü for their helpful comments and suggestions.

Moreover I thankfully acknowledge TUBITAK for financial support during this project ($111T318$).

I would like to appreciate deeply to my colleagues and also roommates Ozan Arı, Mehmet Yağmurcukardeş and Cihan Bacaksız for their all kind of support and warm friendship. Thanks to each of my friends at Izmir Institute of Technology for providing a great atmosphere and a wonderful workplace.

Personally, my special thanks go to my mother Leyla İyikanat and my sister Gözde İyikanat for their ceaseless support, motivation and believing in me. I always need them by my side.

Finally, I would like to thank Elif Özçeri, who never fails to remind me that there is more to life than physics alone.

ABSTRACT

CALCULATIONS OF ELECTRIC AND MAGNETIC PROPERTIES OF TRIANGULAR GRAPHENE FRAGMENTS USING DENSITY FUNCTIONAL THEORY: EFFECTS OF EDGE FUNCTIONALIZATION AND ELECTRIC FIELD

The triangular graphene flakes (*N*-TGFs) we consider have equilateral triangular shapes with zigzag edges, where *N* denotes the number of edge hexagonal cells in one side of the triangle. Termination of these *N*-TGF structures with several elements (of the first two rows of the periodic table) and application of electric field to these flakes alter their electronic and magnetic properties.

In accordance with previous studies [1, 2], it is found that bare flakes have large spin magnetic moment values of $4(N-1)\ \mu_B$, whereas they reduce to $(N-1)\ \mu_B$ for full saturation of edges with Hydrogen, Lithium, Beryllium or Flour atoms. Moreover we have studied possible termination of TGF with other elements like Boron, Carbon and Nitrogen. Hydrogen and Flour atoms prefer to bind at the *top* of an edge Carbon atom. Unlike Hydrogen and Flour, the other atoms prefer to bind at the *bridge* sites.

Recent studies [3, 4] have shown that the magnetic moments of triangular graphene flakes can be controlled by applied electric field. We show that the value of total spin polarization of triangular graphene flakes can be changed by tuning an applied in-plane external field. We demonstrate that, in these flakes total spin polarization can be reduced stepwise with the applied field. The electric field control of ferromagnetism in TGFs promises a new route for spintronic applications.

ÖZET

ÜÇGEN GRAFEN PARÇALARININ ELEKTRİK VE MANYETİK ÖZELLİKLERİNİN YOĞUNLUK FONKSİYONELİ KURAMI HESAPLARI: KENAR FONKSİYONELLEŞTİRME VE ELEKTRİK ALAN ETKİLERİ

İncelediğimiz üçgen grafen parçalar (*N*-ÜGP), zigzag kenarlı eşkanar üçgen şeklindedir, *N* üçgenin bir kenarındaki altıgen hücre sayısını temsil etmektedir. Bu *N*-ÜGP yapıların çeşitli elementler (periyodik tablonun ilk iki sırası) ile sonlandırılması ve bu parçalara elektrik alan uygulanması, bu yapıların elektronik ve manyetik özelliklerini değiştirmektedir.

Önceki çalışmalarla [1, 2] uyumlu bir şekilde, yalın parçaların sahip olduğu $4(N-1)\ \mu_B$' lik yüksek spin manyetik moment değerinin, kenarları Hidrojen, Flor, Lityum ve Berilyum atomları ile tamamen doyurulduğunda $(N-1)\ \mu_B$ değerine düştüğü bulundu. Ayrıca, ÜGP'ların Boron, Karbon ve Nitrojen gibi diğer atomlar ile olası doyurulmalarını da çalıştık. Hidrojen ve Flor atomları kenar karbon atomlarına *tepe* durumda bağlanmayı tercih etmektedirler. Hidrojen ve Flor doyurulmasından farklı olarak, diğer atomlar *köprü* durumunda bağlanmayı tercih ediyorlar.

Son yapılan çalışmalar [3, 4] göstermiştir ki elektrik alan uygulanarak üçgen grafin parçalarının manyetik momentleri kontrol edilebilir. ÜGP'ların toplam spin polarizasyonlarının, düzlemi yönünde uygulanan elektrik alanı ile değiştirilebileceğini gösterdik. Uygulanan alan ile bu grafin parçalarının toplam spin polazisyonlarının adım adım düşürülebileceği gösterildi. ÜGP'lardaki ferromanyetizmanın elektrik alan ile kontrol edilmesi, spintronik uygulamalarında umut verici yeni bir yol vaat etmektedir.

TABLE OF CONTENTS

LIST OF FIGURES

LIST OF TABLES

Table **Page**

CHAPTER 1

INTRODUCTION

Conventional electronic devices are based on the electrical transport of electrons, through a semiconductor, typically slicon based. But existing charge based micro electronic have several disadvantages. First storing charges for a long time is very difficult unless a voltage is continuously applied to keep capacitors charged. Thus, before a computer is turned off, all the work is saved on the hard disc. On the other hand, convetional circuit boards use a lot of energy and generate a lot of heat, limiting chip makers in how closely they can pack circuits together to avoid overheating. Furthermore, as circuits are rapidly miniaturized to squeeze more processing power into a smaller package, the rules of quantum mechanics begin to take over; consideration of all relevant microcopic degrees of freedom, including spin, becomes inevitable.

Spintronics, is one of the solutions to overcome these problems. This new generation of electronic is vastly smaller, faster and more power-efficient relative to conventional one. In Orsay 1988, giant magnetoresistence (GMR) effect [5] in metallic magnetic multilayers, was discovered by Albert Fert and Peter Grünberg, which is considered to be the beginning of spintronics. The discovery of the GMR effect has been awarded with the Nobel Prize in 2007. GMR is the large change in the electrical resistance of a multilayer composed of alternating ferromagnetic and nonmagnetic layers when strong magnetic field applied. The GMR effect give a high resistance if the magnetizations in the ferromagnetic layers are oppositely aligned and low resisdence if they are alligned. The GMR effect evidences that spin-polarized electrons can be transferred through a nonmagnetic material with preserved spin coherence.

Like conventional electronics, spintronics uses the flow of electronics to represent signals and logic states. But while conventional electronics depends on the electrical charge of the electron, spintronics involves angular momentum of electrons, also better known as spin. Placing an electron in a magnetic field results in a coupling of its magnetic moment to the magnetic field. If now the spin is measured we obtain only two possible states, the spin-up state and the spin-down state. This last spintronic property can be used to perform Boolean logic operations, in a similar way as is already done in nowadays computer chips. For this type of logic operations two states are needed, a zero and a one state. This can be easily found in a spintronic device just by assigning the spin-down

state to the zero and the spin-up state to the one state. However, to be able to create a computer chip containing only spintronic devices it is necessary to build fundamental spintronic devices in which the spin state can be manipulated. Carbon based nonmagnetic nanostructures can be useful for spin state manipulation.

Reports of magnetism at room temperature in carbon based structures have stimulated much experimental [6–8] and theoretical [9–11] research work on the magnetic properties of all-carbon systems. Metal-free magnetism is the subject of intense research, because of carbon may provide an easy way for coherent spin manipulation[12] and for building moleculer-based electronic devices. The main advantage of these magnets is that their magnetic and electronic properties can be tuned by moleculer design. Other advantages include conductivity ranging from semi-conducting to insulating, low weight, low temperature processing, low enviromental contamination etc.

Recently, a new kind of carbon materials named as graphene, has been fabricated [13]. Graphene is a monolayer of carbon atoms packed into a dense honeycomb crystal structure. Graphene has proved to have exceptional properties including very fast electron transport [14, 15], room temperature quantum hall effect[16], the highest mechanical strenght[17], and greatest thermal conductivity [18]. Furthermore graphene is a promising candidate for spintronics with very long spin relaxation time [19, 20]. While ideal graphene is non-magnetic itself, many of its derivative materials and nanostructures show various scenarios of magnetism. These include graphene nanoribbons and graphene nano flakes, which can be fabricating by cutting graphene sheets using electron beam irradiation and etching techniques [21, 22]. Magnetism in these nanostructures is usually rather localized along the edge atoms. Although the edge carbon atoms of zigzag edged graphene nanoribbons couple ferromagnetically within the edge, they couple antiferromagnetically across the edges, resulting in no magnetic moment in the system [23, 24]. There are many types of graphene nano flakes like benzene, zigzag edged triangular graphene flakes, armchair edged triangular graphene flakes, zigzag edged hexagonal graphene flakes, armchair edged triangular graphene flakes etc. Among them, zigzag edged triangular graphene flakes, due to their special geometry configuration, they exhibit challenging electronic and magnetic properties. In the zigzag edged triangular graphene flakes magnetic coupling between the zigzag edges are ferromagnetic [25–27], and the non-equivalent sublattices A and B lead to a size dependent magnetic moment [28]. It has been predicted that the net magnetic moments in these nanostructures are usually satisfied with Lieb's theorem [29].

The control of magnetism in these nanostructures is extremely important for spin-

tronic applications. Recent studies have shown that magnetism of triangular graphene flakes can be alter with appliying in-plain or perpendicular electric fields, edge functionalzition with hydrogen atom and defects. However the origin of magnetism in pure carbon nanostructures has not been understood to high satisfaction.

CHAPTER 2

MATERIAL

2.1. Carbon Atom

Carbon is a group IV element in the periodic table with the symbol C and its atomic number is 6. It has six electrons, two of them fill the inner shell 1s which called core electrons and four of them occupy the outer shell of 2s and 2p orbitals which called valance electrons. Therefore carbon atoms ground state electron orbital configuration is $1s^2 2s^2 2p^2$. In the presence of other atoms, carbon atoms prefer excite one electron from the 2s to third 2p orbital, in order to form covalent with the other atoms. Thus the excited state electron configuration is $1s^2 2s^1 2p^3$. The ground and excited state configurations can be seen from Figure 2.1.

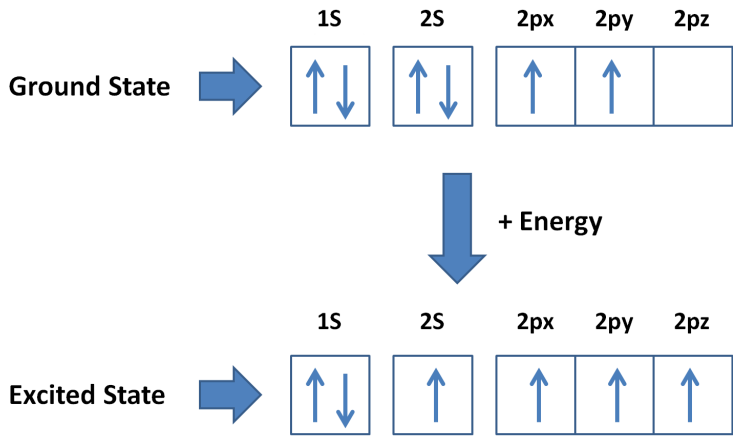

Figure 2.1. Ground and excited state electron orbital configurations of C atom

Allotropes are different structural forms of the same element and can exhibit quite different physical properties. Although diamond and graphite allotropes of carbon, diamond is highly transparent, while graphite is opaque and black. Diamond is among the hardest materials known, while graphite is soft enough to form a streak on paper. Recently, some of the carbon allotropes have attracted a large amount of research and interest. This is partly driven by the promise of new technological applications, some of which have been already demonstrated in the laboratories.

2.1.1. Hybridization of Carbon Atom

Carbon has many allotropes because of the variety of hybridization. Carbon atoms have the ability to bond atoms with sp, sp^2, and sp^3, hybrid orbitals.

- **sp Hybridization:** In the sp hybridization, s orbital and one of the p orbitals are combined together to make two hybrid orbitals. Those hybrid orbitals form a straight line. There is a 180 degree angle between one orbital and the other orbital. Because this type of sp hybridization only uses one of the p orbitals, there are still two p orbitals left which the carbon can use. In the sp hybridization, sp orbitals can be presented as;

$$\Psi_1 = \frac{1}{\sqrt{2}}\Big(\phi_{2s} + \phi_{2p_x}\Big) \tag{2.1}$$

$$\Psi_2 = \frac{1}{\sqrt{2}}\Big(\phi_{2s} - \phi_{2p_x}\Big) \tag{2.2}$$

- **sp^2 Hybridization:** Another kind of hybridization uses the s orbital and two of the p orbitals to form three hybrid orbitals. In this type of hybridization, the three bonds lie on the same plane. The geometric arrangement of these three sp^2 hybrid orbitals is in a flat plane with 120 degree angles between them. The remaining p orbital remains unchanged and is perpendicular to the plane of the three sp^2 orbitals. This hybridization type orbitals can be represented as;

$$\Psi_1 = \frac{1}{\sqrt{3}}\phi_{2s} - \sqrt{\frac{2}{3}}\phi_{2p_x} \tag{2.3}$$

$$\Psi_2 = \frac{1}{\sqrt{3}}\phi_{2s} + \sqrt{\frac{2}{3}}\Big(\frac{\sqrt{3}}{2}\phi_{2p_y} + \frac{1}{2}\phi_{2p_x}\Big) \tag{2.4}$$

$$\Psi_3 = -\frac{1}{\sqrt{3}}\phi_{2s} + \sqrt{\frac{2}{3}}\Big(-\frac{\sqrt{3}}{2}\phi_{2p_y} + \frac{1}{2}\phi_{2p_x}\Big) \tag{2.5}$$

- **sp^3 Hybridization:** In sp^3 hybridization, orbitals are formed by mixing together the $2s$, $2p_x$, $2p_y$, and $2p_z$ atomic orbitals. Diamond is the best example of the material

having this structure. These four sp^3 hybrid orbitals, can be presented as;

$$\Psi_1 = \frac{1}{2}\Big(\phi_{2s} + \phi_{2p_x} + \phi_{2p_y} + \phi_{2p_z}\Big) \tag{2.6}$$

$$\Psi_2 = \frac{1}{2}\Big(\phi_{2s} - \phi_{2p_x} - \phi_{2p_y} + \phi_{2p_z}\Big) \tag{2.7}$$

$$\Psi_3 = \frac{1}{2}\Big(\phi_{2s} - \phi_{2p_x} + \phi_{2p_y} - \phi_{2p_z}\Big) \tag{2.8}$$

$$\Psi_4 = \frac{1}{2}\Big(\phi_{2s} + \phi_{2p_x} - \phi_{2p_y} - \phi_{2p_z}\Big) \tag{2.9}$$

2.2. Carbon Magnetism

Conventional magnetic materials are mostly based on elements with 3d and 4f electrons. In the absence of an external magnetic field, among the periodic table elements only Fe, Co, and Ni exhibit spontaneous ferromagnetism at room temperature. The magnetic properties of these elements originate from the partially filled orbitals.

On the other side, recent studies have shown that various materials which have only s and p orbitals exhibit magnetic behavior. Due to low density, low production costs and biocompatibility light elements based on magnetism, have attracted considerable attention for possible applications in modern technology. Observations of magnetism in various carbon systems [30–32] have stimulated much experimental and theoretical research work but the origin of magnetism in pure carbon nanostructures has not been understood to high satisfaction. In this thesis various carbon nanostructures have been investigated to understand the nature of carbon magnetism.

2.3. Graphene

Graphene is a flat monolayer of carbon atoms tightly packed into a two dimensional honeycomb lattice. It can be wrapped up into 0D fullerenes, rolled into 1D nanotubes or stacked into 3D graphite [33]. The tight binding calculation of the graphene band structure at low energies, was first deduced by Wallace in 1947 [34]. For more than 60 years, researchers have tried to find it since it has been predicted to have peculiar electronic properties.

Finally in 2004, Andre Geim, Kostya Novoselov, and their co-workers at University of Manchester, managed to isolate a few-layer and monolayer of graphene from

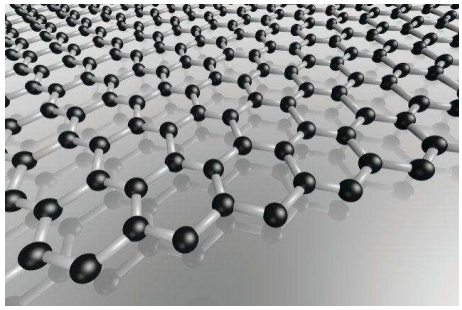

Figure 2.2. Graphene

graphite bulk with simple Scotch-tape method [13]. After its isolation as a single layer, graphene has become a topic of great interest to the scientific community due to its peculiar properties.

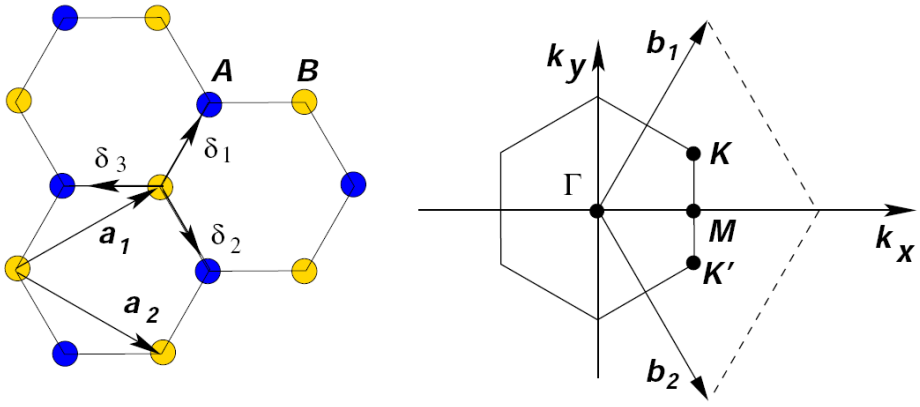

Figure 2.3. Honeycomb lattice and its Brillouin zone. $\mathbf{a_1}$, $\mathbf{a_2}$ are the lattice unit vectors, $\mathbf{b_1}$, $\mathbf{b_2}$ corresponding reciprocal lattice vectors and δ_i, i=1,2,3 are the nearest neighbour vectors. Adapted from Ref. [35].

2.3.1. Lattice Structure of Graphene

The honeycomb lattice of graphene, as shown in Figure 2.3, consists of two non-equivalent sublattices denoted as A and B. In one unit cell, it has two identical carbon atoms, one of them belongs to A sublattice and the other belongs to B sublattice. The two lattice vectors can be expressed as;

$$\mathbf{a_1} = a\Big(\frac{3}{2}, \frac{\sqrt{3}}{2}\Big), \quad \mathbf{a_2} = a\Big(\frac{3}{2}, -\frac{\sqrt{3}}{2}\Big). \tag{2.10}$$

The nearest neighbour distance (carbon-carbon distance) is represented by the letter *a* in equation and is approximately 1.42 Å. The corresponding reciprocal lattice vectors $\mathbf{b_1}$ and $\mathbf{b_2}$ are defined by the condition $\mathbf{a_i}\ \mathbf{b_j} = 2\pi\delta_{ij}$ are then:

$$\mathbf{b_1} = \frac{2\pi}{a}\Big(\frac{1}{3}, \frac{\sqrt{3}}{3}\Big), \quad \mathbf{b_2} = \frac{2\pi}{a}\Big(\frac{1}{3}, -\frac{\sqrt{3}}{3}\Big). \tag{2.11}$$

The corresponding first Brillouin zone is shown in Figure 2.3. This first Brillouin zone has the same form as the original hexagonal honeycomb lattice of graphene, but rotated with respect to them by $\pi/2$. The six points at the corners of first Brillouin zone can be divided into two groups of three which are equivalent. Thus, we only need to consider the most important two points K and K' at the corners of the graphene first Brillouin zone. These two points are named Dirac points. Explicitly, their positions in momentum space are given by:

$$\mathbf{K} = \frac{2\pi}{a}\Big(\frac{1}{3}, \frac{1}{3\sqrt{3}}\Big), \quad \mathbf{K'} = \frac{2\pi}{a}\Big(\frac{1}{3}, -\frac{1}{3\sqrt{3}}\Big). \tag{2.12}$$

Then nearest neighbour vectors (in real space) are

$$\delta_{\mathbf{1}} = \frac{a}{2}\Big(1, \sqrt{3}\Big), \quad \delta_{\mathbf{2}} = \frac{a}{2}\Big(1, -\sqrt{3}\Big), \quad \delta_{\mathbf{3}} = -a\Big(1, 0\Big). \tag{2.13}$$

2.3.2. Band Structure of Graphene

The first calculation of the electronic properties of graphene dates back to 1947 when P. R. Wallace calculated the electronic dispersion of graphene [34]. The electrical properties of graphene can be described by a tight-binding model. In this model the energy of the electrons is;

$$E(\mathbf{k}) = \pm\gamma\sqrt{1 + 4\cos^2(\frac{k_x a}{2}) + 4\cos(\frac{k_x a}{2})\cos(\frac{\sqrt{3}k_y a}{2})}. \tag{2.14}$$

The dispersion relation is plotted in Figure 2.4 . It can be seen from figure the Fermi level at E($\mathbf{k}$) = 0 is reached by six corners of the first Brillouin zone, among which

there are only two inequivalent points (Dirac points) due to the periodicity of the reciprocal lattice.

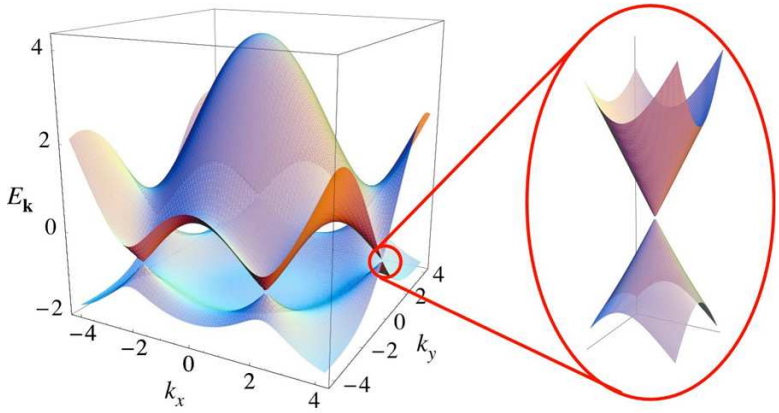

Figure 2.4. Energy dispersion in the honeycomb lattice. Energy is in the units of t where t = 2.7 eV. Adapted from Ref. [35].

As shown in Figure 2.4, the dispersion relation close to the Dirac points can be linearised. Let us take one of the Dirac points, say $\mathbf{K}$, and make an expansion around it, $\mathbf{k} = \mathbf{K} + \mathbf{q}$, for small $\mathbf{q}$ compared to $\mathbf{K}$ we find:

$$E(\mathbf{K} + \mathbf{q}) = E(\mathbf{q}) \approx \pm v_F \hbar |\mathbf{q}|. \tag{2.15}$$

2.3.3. Spin Order in Graphene

While ideal graphene is non-magnetic itself, many of its derivative materials and nanostructures, show various scenarios of magnetism. Graphene shows magnetic properties when single layer of graphene cut properly [1, 2, 36] or removed carbon atoms from lattice structure [37, 38].

To understand the magnetism in graphene we should examine the honeycomb lattice structure of graphene which have been shown in Figure 2.5. Graphene can be viewed as bipartite lattice composed of two interpenetrating triangular sublattices. Thus, such lattice with a basis contains two identical carbon atoms per primitive unit cell. A bipartite lattice can be partitioned into two mutually interconnected sublattices A and B. Each atom belonging to sublattice A is connected to the atoms in sublattice B only, and vice versa.

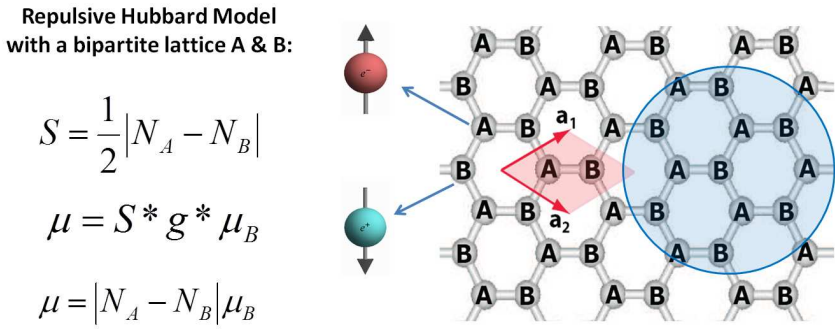

Figure 2.5. Graphene's lattice structure. Blue and red carbon atoms denotes different sublattice atoms of graphene.

Orbital structures of carbon atoms in graphene is shown in Figure 2.6. All carbon atoms make three σ bond with nearest neighbours, while leaving behind a p_z-orbital electron contributing to the spin magnetic moment. These p_z-orbital electrons in each sublattice have opposite spin states and make spin paired π bonds. Due to there is a A sublattice electron for every B sublattice electron, magnetic contribution vanish for graphene. Difference in the numbers of electrons of the A and B sublattices leads to magnetic moments in the properly cuted graphene edge and vicinity of vacancy sites in graphene.

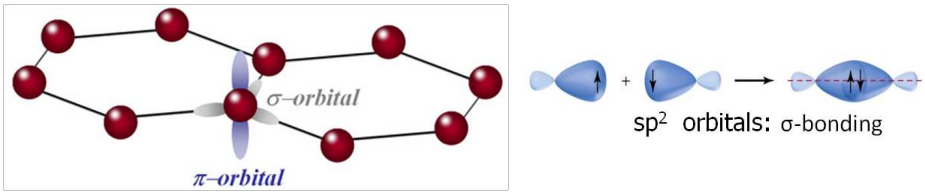

Figure 2.6. Orbital structures of carbon atoms in graphene.

To understand clearly magnetism in graphene we should look Lieb's theorem. Lieb derived stronger results for the exactly half-filled Hubbard model. Lieb's theorem [29] determines the total spin of a bipartite system described by the Hubbard model. This theorem states that in the case of repulsive electron-electron interactions, a bipartite system at half-filling has the ground state characterized by the total spin;

$$S = \frac{1}{2}\Big|N_A - N_B\Big|, \tag{2.16}$$

where N_A and N_B are the numbers of sites in sublattices A and B, respectively. The ground state is unique and the theorem holds in all dimensions without the necessity of a periodic lattice structure. For example, the total spin of the graphene fragment which is

shown in Figure 2.5 is;

$$S = \frac{1}{2}\Big|N_A - N_B\Big| = \frac{1}{2}\Big|7 - 4\Big| = 1.5. \tag{2.17}$$

Using with the calculations which given in Figure 2.5 we find that total magnetic moment of this fragment is 3 μ_B.

2.4. Graphene Based Magnetic Nanostructures

2.4.1. Graphene Nanoribbons (GNRs)

Graphene is a zero bandgap material. In order to use graphene in semiconductor electronics, its very important to open a band gap. One of the methods to increase the band gap of graphene is to form graphene nanoribbon (GNR).

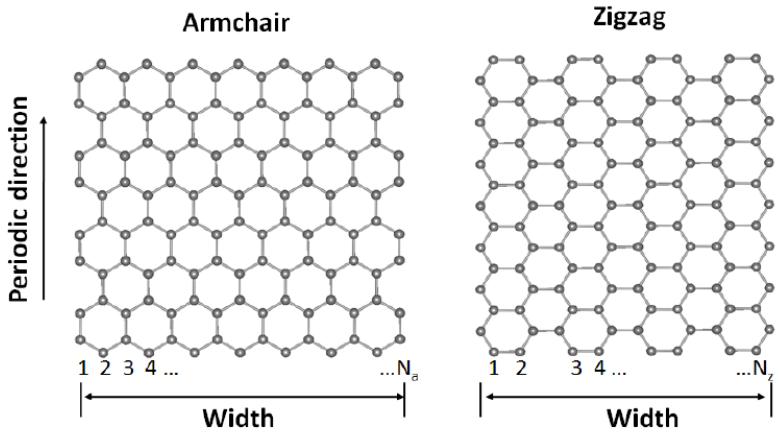

Figure 2.7. Structure of armchair and zigzag nanoribbons. Adapted from Ref. [39]

GNRs, are strips of graphene with ultra-thin width (<50 nm). Their structures and their electronic and magnetic properties have been subject of interest both experimentally [40, 41] and theoritically [42–44]. There are two main shapes for graphene nanoribbon edges, namely armchair edges GNR (AGNR) and zigzag edges GNR (ZGNR) which can be seen from Figure 2.7. Although the pristine infinite graphene sheet is nonmagnetic ZGNR is theoretically predicted to be magnetic with two spin-polarized edge states, which are ferromagnetically coupled in the same edge, but antiferromagnetically cou-

pled between two opposite edges, while the armchair edge GNR (AGNR) is found to be nonmagnetic [36]. The magnetic structure of ZGNR shown in Figure 2.8.

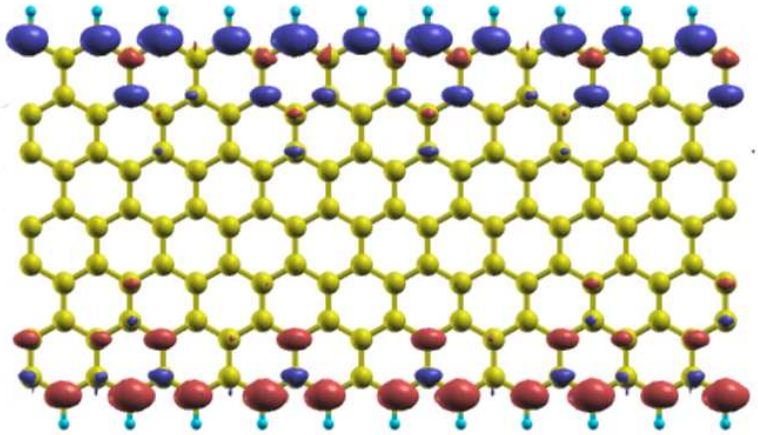

Figure 2.8. Isosurfaces of charge density difference of spin-up (↑) and spin-down (↓) for ZGNR

2.4.2. Graphene Nano Flakes (GNFs)

Graphene nano flake (GNF) can be synthesized by cutting the graphene sheet [45, 46]. Pristine graphene has continuous band structure with zero band gap whereas GNFs have discrete, molecular energy levels with tunable band gap (see Figure 2.9). GNFs are a nanometer-size fragment of graphene which has a closed edge. Understanding the properties of GNFs is important because they are candidates of future carbon-based nanoelectronics and spintronics alternative to silicon devices. Compared to graphene and GNRs, GNFs have additional advantages in their electronic and magnetic properties. These additional advantages arise because GNFs not only have edge states, but also corner states, and may also be cut into a much larger variety of different shapes. There are many types of regular GNFs, as displayed in Figure 2.10.

Magnetic properties of GNFs are deeply depend on flakes shape. For example while square and hexagonal shaped GNFs do not have net magnetic moment, zig-zag edged triangular graphene flakes (TGFs) exhibit magnetic structure. In TGFs, the spin alignments on their all edges couple ferromagnetically. The total magnetic moment obeys Lieb's theorem, and can be tuned by changing the size of TGF [28]. Due to these interesting properties, in this thesis electronic and magnetic properties of TGFs examined.

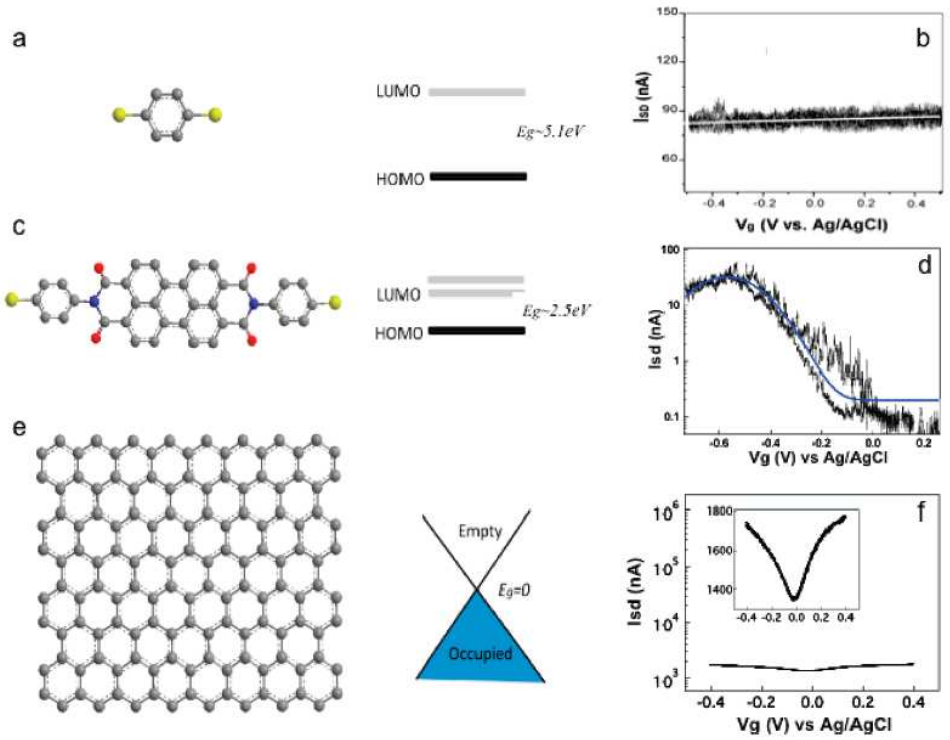

Figure 2.9. Molecular structures, energy diagrams, and electrochemical gate effects of benzenedithiol, PTCDI, and a graphene sheet:(a) Benzenedithiol (containing a single benzene ring) has a large LUMO-HOMO gap (5.1 eV) and is 'insulating' with a weak gate effect (b). (c) The LUMO-HOMO gap of PTCDI (containing seven rings) is $\sim$ 2.5eV, and the molecule is 'semiconducting' with a large gate effect (d). (e) Graphene (containing a large number of rings) has a zero energy gap between the conduction and valence bands and shows semimetallic behavior with a weak gate effect (f). Adapted from Ref. [47].

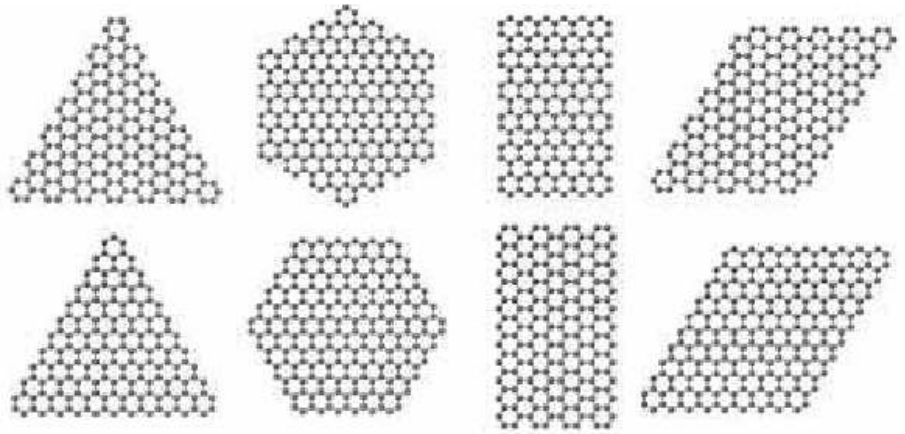

Figure 2.10. Basic geometric structures of typical GNFs. At the above armchair edged GNFs, at the below zigzag edged GNFs. Adapted from Ref. [39].

CHAPTER 3

THEORETICAL BACKGROUND

3.1. Electronic Structure Calculations

Understanding the physical and chemical properties of matter is an advanced many-body problem. In general, we examine collection of particles interacting through electrostatic interactions. We can write the hamiltonian of such a system in the following general form:

$$\hat{H} = -\hbar^2 \sum_{I=1} \frac{\nabla_{\mathbf{I}}^{\mathbf{2}}}{2M_I} - \hbar^2 \sum_{i=1} \frac{\nabla_{\mathbf{i}}^{\mathbf{2}}}{2m_i} - \sum_{i,I} \frac{Z_I e^2}{|\mathbf{r_i} - \mathbf{R_I}|} + \frac{1}{2} \sum_{i \neq j} \frac{e^2}{|\mathbf{r_i} - \mathbf{r_j}|} + \frac{1}{2} \sum_{I \neq J} \frac{Z_I Z_J e^2}{|\mathbf{R_I} - \mathbf{R_J}|} \tag{3.1}$$

where lower case subscripts denote electrons, and upper case subscripts denote nuclei. Z_I is the atomic number of the nucleus. In principle all the properties can be derived by solving the many-body Schrödinger equation:

$$\hat{H}\psi_i(\mathbf{r}, \mathbf{R}) = \mathbf{E_i}\psi_{\mathbf{i}}(\mathbf{r}, \mathbf{R}). \tag{3.2}$$

In practise, this problem is almost impossible to solve exactly except for a few simple cases. This requires simplifications to the hamiltonian which involves several approximations.

The first approximation is the pseudopotential approximation. In this approximation electrons can be divided in two categories: valence and core electrons, according to their position in an atom. The core electrons are not directly responsible for determining the properties of the elements. Unlike the core electrons, most physical properties of solids are dependent on the valence electrons. It is for this reason that the pseudopotential approximation is introduced. This approximation uses this fact to remove the core electrons and the strong nuclear potential and replace them with a weaker pseudopotential

which acts on a set of pseudo wavefunctions rather than the true valence wavefunctions. Figure 3.1 shows the electronic wave functions, and generated pseudo wavefunction and corresponding potentials.

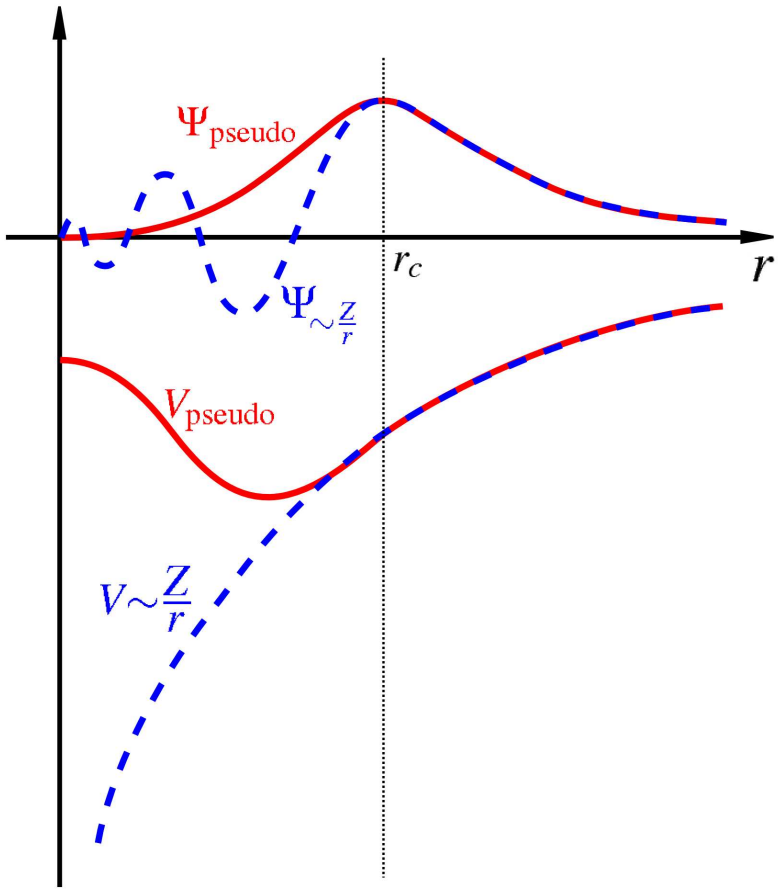

Figure 3.1. Sketch of the all-electron and pseudo potentials and their corresponding wave functions. The radius at which all-electron and pseudo potentials match is displayed as r_c. Adapted from Ref. [48].

A pseudopotential is not unique, therefore several methods of generation also exist. However they must obey several criteria. These are:

1. The core charge produced by the pseudo wavefunctions must be the same as that produced by the atomic wavefunctions.
2. The pseudo-electron eigenvalues and the valance eigenvalues must be same.
3. Pseudo wavefunctions must be continuous at the core radius as well as its first and second derivative and also be non-oscillatory.
4. The pseudo wavefunctions and atomic wavefunctions must agree beyond the core radius.

Another approximation is the Born-Oppenheimer or adiabatic approximation. The nuclei are much heavier than the electrons which results in the nuclei's moving much slower compared to the electrons. This makes kinetic energy term is negligible and the first term dissappears in the hamiltonian. The last term reduces to a constant. We are left with the kinetic energy of the electrons, the potential energy due to electron-electron interactions and the potential energy of the electrons in the (external) potential of the nuclei. We write this formally as;

$$\hat{H} = \hat{T} + \hat{V} + \hat{V}_{ext}. \tag{3.3}$$

3.2. The Electronic Problem

Many-body electronic Schrödinger equation is still a very difficult problem to handle and exact solution is known only for some simple cases. Alot of approximations have been improved for handle the solution. Fistly in 1920 Douglas Hartree developed an approach named after himself called the Hartree approximation [49]. In this approximation the potential corresponding to electron-electron interactions could be

$$V(\mathbf{r}) = \int \mathbf{dr'} \frac{\mathbf{e^2 n(r')}}{|\mathbf{r} - \mathbf{r'}|} \tag{3.4}$$

where n is number density of electrons

$$n(\mathbf{r}) = \sum_{\mathbf{j}} |\psi_{\mathbf{j}}(\mathbf{r})|^{\mathbf{2}}. \tag{3.5}$$

Then substitution the above potential to the Schrödinger equation we obtain the Hartree equation ;

$$E_l \psi_l(\mathbf{r}) = [\mathbf{T_{elec}} + \mathbf{V_{ion}}(\mathbf{r}) + \mathbf{V}(\mathbf{r})]\psi_{\mathbf{l}}(\mathbf{r}). \tag{3.6}$$

In fact, Hartree approximation is wrong. It does not recognize the Pauli principle. According to Pauli exclusion principle, two electrons, cannot occupy the state all of their quantum numbers are the same. The true many-body wave function must vanish whenever two electrons occupy the same position, but the Hartree wave function cannot have this

property. If we want to hold Pauli exclusion principle total electron wave function should be in an antisymmetric form;

$$\Psi = \frac{1}{\sqrt{N!}} \begin{vmatrix} \psi_1(\mathbf{r_1}, \sigma_\mathbf{1}) & \psi_1(\mathbf{r_2}, \sigma_\mathbf{2}) & ... & \psi_1(\mathbf{r_N}, \sigma_\mathbf{N}) \\ \psi_2(\mathbf{r_1}, \sigma_\mathbf{1}) & \psi_2(\mathbf{r_2}, \sigma_\mathbf{2}) & ... & \psi_2(\mathbf{r_N}, \sigma_\mathbf{N}) \\ \psi_3(\mathbf{r_1}, \sigma_\mathbf{1}) & \psi_3(\mathbf{r_2}, \sigma_\mathbf{2}) & ... & \psi_3(\mathbf{r_N}, \sigma_\mathbf{N}) \\ . & . & ... & . \\ . & . & ... & . \\ \psi_N(\mathbf{r_1}, \sigma_\mathbf{1}) & \psi_N(\mathbf{r_2}, \sigma_\mathbf{2}) & ... & \psi_N(\mathbf{r_N}, \sigma_\mathbf{N}) \end{vmatrix}$$

which is known as a slater determinant [50]. Where $\psi_i(\mathbf{r_j}, \sigma_\mathbf{j})$ is the single-electron spin orbital, and it is the product of position $\phi_i(\mathbf{r_i})$ and spin $\alpha_i(\sigma_i)$ component. This approximation is called as a Hartree-Fock (HF) [51].

The Slater determinant above is helpful in obtaining the exchange term. Appliying exchange term to the Hartree equation leads to the Hartree-Fock equation:

$$E_l\psi_l(\mathbf{r}) = [\mathbf{T_{elec}} + \mathbf{V_{ion}}(\mathbf{r}) + \mathbf{V}(\mathbf{r})]\psi_\mathbf{l}(\mathbf{r}) - \frac{\mathbf{1}}{\mathbf{2}} \sum_\mathbf{j} \int \mathbf{d^3r'} \psi_\mathbf{j}^*(\mathbf{r'}) \psi_\mathbf{i}(\mathbf{r'}) \frac{\mathbf{1}}{|\mathbf{r} - \mathbf{r'}|} \psi_\mathbf{j}(\mathbf{r}) \quad (3.7)$$

The Hartree-Fock equations deal with exchange exactly; however, the equations neglect more detailed correlations due to many-body interactions. The effects of electronic correlations are not negligible. This is first failure of HF approximation. On the other hand since wave-function methods in general limited to molecules with a small number of active electrons, this approximation is not usefull for many-body structures.

In the 1920's Thomas-Fermi developed another approach to this electronic problem. They purposed that, the full electronic density was the fundamental variable of the many-body problem, and derived a differential equation for the density without resorting to one-electron orbitals. But Thomas-Fermi approximation did not include exchange and correlation effects. Both Thomas and Fermi neglected exchange and correlation among the electrons; however, this was extended by Dirac in 1930 [52], who formulated the local approximation for exchange still in use today. This leads to the energy functional for

electrons in an external potential $V_{ext}(\mathbf{r})$

$$E_{TF}[n] = C_1 \int d^3r n(\mathbf{r})^{\frac{5}{3}} + \int d^3r V_{ext}(\mathbf{r}) n(\mathbf{r}) + C_2 \int d^3r n(\mathbf{r})^{\frac{4}{3}} + \frac{1}{2} \int d^3r d^3r' \frac{n(\mathbf{r}) n(\mathbf{r}')}{|\mathbf{r} - \mathbf{r}'|} \tag{3.8}$$

in here the first term is the local approximation to the kinetic energy, the third term is the local exchange and the last term is the classical electrostatic Hartree energy.

However, the Thomas-Fermi approximation is too crude, missing essential physics and chemistry, such as shell structures of atoms and binding of molecules. Although their approximation is not accurate enough for present-day electronic structure calculations, the approach illustrates the way density functional theory works.

3.3. Density Functional Theory

Density functional theory (DFT) is one of the most widely used methods for electronic structure calculations in condensed matter. The reasons of its popularity and success are high computational efficiency and its accuracy. The general idea of DFT is that any property of system which has many interacting particles can be viewed as a functional of the ground state electron density $n_0(\mathbf{r})$ [53, 54]. Although DFT is significant, it underestimates the band gaps of semiconductors and some other electronic properties of highly correlated systems. DFT is based on the famous theorem by Hohenberg and Kohn [53] .

3.3.1. Hohenberg-Kohn Theorems

DFT is based upon two theorems formulated by Hohenberg and Kohn.

- **Theorem 1:** There is a one-to-one correspondence between the ground-state density $n_0(\mathbf{r})$ of a many-electron system and the external potential $V_{ext}(\mathbf{r})$. Thus since the density $n_0(\mathbf{r})$ determines the potential $V_{ext}(\mathbf{r})$, it will determine the ground state energy and all other electronic properties of the system. The problem is now only how to find this density. The second theorem is helpful in this matter.

- **Theorem 2:** The groundstate energy can be obtained variationally: the density that minimises the total energy is the exact groundstate density.

Therefore, the total energy of the systems is a functional of electron density and can be written as:

$$E_{HK}[n] = T[n] + E_{int}[n] + \int d^3r V_{ext}(\mathbf{r})n(\mathbf{r}) + E_{II}$$
$$\equiv F_{HK}[n] + \int d^3r V_{ext}(\mathbf{r})n(\mathbf{r}) + E_{II}, \tag{3.9}$$

where E_{II} is the interaction energy of the nuclei and $F_{HK}[n]$ is the internal energy functional. It should be noted that Hohenberg-Kohn density functional $F_{HK}[n]$ is universal for any many-electron system. So if we know $F_{HK}[n]$ then we can determine the electron density of the ground state by simply minimizing the energy functional.

3.3.2. The Kohn-Sham Equations

The expression of the kinetic energy in terms of the electronic density is not achieved yet. This problem solved by W.Kohn and L.Sham. In 1965, Kohn and Sham [54] proposed that, the exact ground-state density can be represented by the ground-state density of an auxiliary system of non-interacting particles. In this auxiliary system all the interactions between electrons are classified into an exchange-correlation term. Using with the Hartree atomic units $\hbar = m_e = e = \frac{4\pi}{\epsilon_0} = 1$ the auxiliary hamiltonian of the auxiliary independent-particle system is

$$H^{\sigma}_{aux} = -\frac{1}{2}\nabla^2 + V^{\sigma}(\mathbf{r}). \tag{3.10}$$

here $V^{\sigma}(\mathbf{r})$ is a potential acting on an electron with spin σ at point $\mathbf{r}$. And the density of the auxiliary system is given by

$$n(\mathbf{r}) = \sum_{\sigma} n(\mathbf{r}, \sigma) = \sum_{\sigma} \sum_{i=1}^{N^{\sigma}} |\psi_i^{\sigma}(\mathbf{r})|^2. \tag{3.11}$$

where ψ_i^σ is the i-th single particle orbital with spin component σ. The independent-particle kinetic energy T_s is given by

$$T_s = -\frac{1}{2}\sum_\sigma \sum_{i=1}^{N^\sigma} < \psi_i^\sigma | \nabla^2 | \psi_i^\sigma > = \frac{1}{2}\sum_\sigma \sum_{i=1}^{N^\sigma} \int d^3r |\nabla \psi_i^\sigma(\mathbf{r})|^2, \tag{3.12}$$

and we can define the classical Coulomb interaction term as

$$E_{Hartree}[n] = \frac{1}{2}\int d^3r d^3r' \frac{n(\mathbf{r})n(\mathbf{r'})}{|\mathbf{r}-\mathbf{r'}|}. \tag{3.13}$$

Finally we can write the total energy functional as follows,

$$E_{KS} = T_s[n] + \int d\mathbf{r} V_{ext}(\mathbf{r}) n(\mathbf{r}) + E_{Hartree}[n] + E_{II} + E_{xc}[n]. \tag{3.14}$$

$E_{xc}[n]$ contains all many-body effects of exchange and correlation. To derive the Kohn-Sham equations, we must minimise the energy with respect to the charge density n($\mathbf{r}, \sigma$). Because of the independent-particle kinetic energy T_s is explicitly expressed as a functional of the orbitals, one should calculate the gradient of the energy with respect to the orbitals

$$\frac{\delta E_{KS}}{\delta \psi_i^{\sigma *}(\mathbf{r})} = \frac{\delta T_s}{\delta \psi_i^{\sigma *}(\mathbf{r})} + \left[\frac{\delta E_{ext}}{\delta n(\mathbf{r},\sigma)} + \frac{\delta E_{Hartree}}{\delta n(\mathbf{r},\sigma)} + \frac{\delta E_{xc}}{\delta n(\mathbf{r},\sigma)}\right] \frac{\delta n(\mathbf{r},\sigma)}{\delta \psi_i^{\sigma *}(\mathbf{r})} = 0, \tag{3.15}$$

then orthonormalization condition requires

$$< \psi_i^\sigma | \psi_j^{\sigma'} > = \delta_{i,j}\delta_{\sigma,\sigma'}. \tag{3.16}$$

Using expressions 3.11 and 3.12 for $n^\sigma(\mathbf{r})$ and T_s, which give

$$\frac{\delta T_s}{\delta \psi_i^{\sigma *}(\mathbf{r})} = -\frac{1}{2}\nabla^2 \psi_i^\sigma(\mathbf{r}), \tag{3.17}$$

$$\frac{\delta n^\sigma(\mathbf{r})}{\delta \psi_i^{\sigma *}(\mathbf{r})} = \psi_i^\sigma(\mathbf{r}). \tag{3.18}$$

and the Lagrange multiplier method for handling the constraints, this leads to the Khon-Sham Schrödinger-like equations:

$$(H_{KS}^{\sigma} - \epsilon_i^{\sigma})\psi_i^{\sigma}(\mathbf{r}) = 0, \tag{3.19}$$

where ϵ_i^{σ} are Khon-Sham eigen energies. And H_{KS}^{σ} is the effective hamiltonian

$$H_{KS}^{\sigma}(\mathbf{r}) = -\frac{1}{2}\nabla^2 + V_{KS}^{\sigma}(\mathbf{r}), \tag{3.20}$$

where $V_{KS}^{\sigma}(\mathbf{r})$ is Kohn-Sham potential and it is defined by

$$V_{KS}^{\sigma}(\mathbf{r}) = V_{ext}(\mathbf{r}) + \frac{\delta E_{Hartree}}{\delta n(\mathbf{r},\sigma)} + \frac{\delta E_{xc}}{\delta n(\mathbf{r},\sigma)} \tag{3.21}$$

$$= V_{ext}(\mathbf{r}) + V_{Hartree}(\mathbf{r}) + V_{xc}^{\sigma}(\mathbf{r}). \tag{3.22}$$

Equations 3.19-3.22 are called the Kohn-Sham Equations. The solution of the Khon-Sham equations can be achieved by applying the iterative procedure. Some starting density $n_0^{\uparrow}(\mathbf{r})$, $n_0^{\downarrow}(\mathbf{r})$ are guessed, and a hamiltonian $H_{KS1}^{\sigma}(\mathbf{r})$ is constructed with it. The eigenvalue problem is solved, then the densities $n_1^{\uparrow}(\mathbf{r})$, $n_1^{\downarrow}(\mathbf{r})$ handled with it. Most probably $n_1^{\uparrow}(\mathbf{r})$, $n_1^{\downarrow}(\mathbf{r})$ will differ from $n_0^{\uparrow}(\mathbf{r})$, $n_0^{\downarrow}(\mathbf{r})$. Then $n_1^{\uparrow}(\mathbf{r})$, $n_1^{\downarrow}(\mathbf{r})$ are used to construct $H_{KS2}^{\sigma}(\mathbf{r})$, which will yield a $n_2^{\uparrow}(\mathbf{r})$, $n_2^{\downarrow}(\mathbf{r})$, etc. This procedure repeat until $n^{\uparrow}(\mathbf{r})$, $n^{\downarrow}(\mathbf{r})$ is converged. Then using with converged values energy, Hellmann-Feynman forces [55], [56], stresses [57], [58], eigenvalues can be calculated. After Hellmann-Feynmann forces and stresses are calculated the system can be relaxed geometrically [48] and find local minimum around given initial coordinates.

The Kohn-Sham wave functions must be represented as a linear combination of a set of functions, e.g. basis set. Different basis sets maybe more or less convenient for computational efficiency. There are three basic basis sets to be used in Khon-Sham equations: linearized augmented plane waves (LAPWs), linear combinations of atomic orbitals (LCAO), and plane waves. Each method has its advantages and pitfalls. In this thesis LCAO basis set is used for the Khon-Sham wave functions.

3.3.3. Approximations to the Exchange-Correlation Potential

Up to now, except the preceding Born-Oppenheimer approximation, no other approximations were made. But exchange correlation term hasnt explained yet. This term includes all the remaining complicated electronic contributions. The exchange-correlation term is very complex and can not handle simply. However there are several approximations to the exchange correlation, namely local density approximation (LDA), generalised gradient approximation (GGA), Hybrid functionals, LDA+U and Exact Exchange Functionals.

3.3.3.1. Local Spin Density Approximation (LSDA)

The most widely used approximation to handle exchange correlation energy is the local spin density approximation (LSDA). This approximation first formulated by Kohn and Sham [54] in 1965. LSDA approximation is to postulate that the density at each point is the same as that of the homogeneous electron gas. In this approximation the exchange-correlation functional is given by

$$E_{xc}^{LSDA}[n^{\uparrow}, n^{\downarrow}] = \int d^3r n(\mathbf{r}) \epsilon_{xc}(n^{\uparrow}(\mathbf{r}), n^{\downarrow}(\mathbf{r})), \tag{3.23}$$

where $\epsilon_{xc}(n^{\uparrow}(\mathbf{r}), n^{\downarrow}(\mathbf{r}))$ is the exchange-correlation energy per particle of a homogeneous electron gas. $\epsilon_{xc}(n^{\uparrow}(\mathbf{r}), n^{\downarrow}(\mathbf{r}))$ can be written as the sum of exchange and correlation contributions

$$\epsilon_{xc}(n^{\uparrow}(\mathbf{r}), n^{\downarrow}(\mathbf{r})) = \epsilon_x(n^{\uparrow}(\mathbf{r}), n^{\downarrow}(\mathbf{r})) + \epsilon_c(n^{\uparrow}(\mathbf{r}), n^{\downarrow}(\mathbf{r})), \tag{3.24}$$

where the exchange part $\epsilon_x(n^{\uparrow}(\mathbf{r}), n^{\downarrow}(\mathbf{r}))$ can be expressed explicitly

$$\epsilon_{xc}(n^{\uparrow}(\mathbf{r}), n^{\downarrow}(\mathbf{r})) = -\frac{1}{2^{\frac{2}{3}}}\frac{3}{8}e^2 \left(\frac{3}{\pi} n^{\uparrow}(\mathbf{r})\right)^{\frac{1}{3}} - \frac{1}{2^{\frac{2}{3}}}\frac{3}{8}e^2 \left(\frac{3}{\pi} n^{\downarrow}(\mathbf{r})\right)^{\frac{1}{3}}. \tag{3.25}$$

For the correlation part $\epsilon_c(n^{\uparrow}(\mathbf{r}), n^{\downarrow}(\mathbf{r}))$, there is no such explicit expression. But

there are highly accurate Quantum Monte Carlo calculations for the homogeneous electron gas [59]. The LSDA is very successful an approximation for many systems of interest, it gives a very good results especially for transition metals due to the fact that the electron density varies smoothly. But LSDA's results become worse with increasing inhomogeneity.

3.3.3.2. Generalized Gradient Approximation (GGA)

The Generalized Gradient Approximation (GGA) uses not only the density n(**r**) at a particular point, but also its gradient $\nabla n(\mathbf{r})$, in order to account for the non-homogeneity of the true electron density. In GGA exchange-correlation energy can be written as follows,

$$E_{xc}^{LSDA}[n^{\uparrow}, n^{\downarrow}] = \int d^3r n(\mathbf{r}) \epsilon_{xc}(n^{\uparrow}(\mathbf{r}), n^{\downarrow}(\mathbf{r}), \nabla n^{\uparrow}(\mathbf{r}), \nabla n^{\downarrow}(\mathbf{r})). \tag{3.26}$$

Widely used GGA's can now provide the accuracy required for density functional theory to be used in various type of analysis. Generally GGA approximation improves atomic energies, binding energies, bond lengths and bond angles when compared the ones obtained by LDA. In this thesis all of the calculations are carried out with GGA.

3.4. Method

Optimization of geometrical structures of triangular graphene flakes and calculations of their magnetic and electric properties are performed by using the software package SIESTA based on densiy functional theory (DFT). The exchange-correlation potential has been approximated by generalized gradient approximation (GGA). For geometry optimizations, the conjugate gradient algorithm and the convergence criteria of 0.04 eV/Åand 10^{-5} eV for the forces and total energies, respectively, were applied. The electrostatic potentials were determined on a real-space grid with a mesh cutoff energy of 300 Ry. We make use of norm-conserving Troullier Martins pseudopotentials and a double-zeta basis set composed of numerical atomic orbitals of finite range. The Brillouin zone has been sampled with (1, 1, 1) points within the Monkhorst-Pack k-point sampling scheme.

CHAPTER 4

EDGE FUNCTIONALIZATION OF TGF

4.1. Introduction

While ideal graphene is non-magnetic itself and it has zero-band gap around the fermi level, many of its derivative materials and nanostructures, show various scenarios of magnetism and they have tunable band gap. These nanostructures which are a zero dimensional dots, can be synthesized by cutting the graphene sheets [45, 46] are called graphene nano flakes. Understanding the properties of graphene nano flakes is motivated by the fact that the basic components of future electronics or spintronics devices need to be at the nanometer scale.

The electronic and magnetic properties of graphene nano flakes depend strongly on their shapes and edges [1, 60–62]. One of the most important and familiar graphene nano flake is zigzag edged triangular graphene flakes (TGFs). In the TGFs the magnetic ordering among the zigzag edges is ferromagnetic, and the presence of non-equivalent sublattices A and B leads a magnetic moment [25, 27, 63]. It is predicted that the net magnetic moments of these TGFs are usually compatible with Lieb's theorem [29]. Unlike conventional magnetic materials which magnetism is due to d or f electrons, magnetism in the TGFs orginates from the p electrons, display weak spin-orbit and hyperfine couplings which are the main channels of relaxation and decoherence of electron spins [24, 64, 65]. These interesting properties provides opportunities for designing spintronic systems with TGFs as the building block.

However, to use these TGFs in spintronic devices it is necessary to be able to alter their spin states. Earlier experimental observations [46, 66] and theoretical studies [60, 67–69] show that the electronic and magnetic properties of graphene based fragments can be altered significantly upon the termination of their edges. Furthermore, recent studies show that the electronic and magnetic properties of TGFs can be changed notably with size, edge termination [28], and subsitutional doping [68]. With these motivations, the main aim of this chapter is to clearly understand, the edge effect of functionalization on the control and manipulation of magnetic and electronic properties of TGFs.

In this chapter edge functionalization of TGFs with Hydrogen, Flourine, Lithium, Berillium, Boron, Carbon and Nitrogen are considered in order to observe the effect of

different elements on the electronic and magnetic properties of TGFs. In accordance with a previous study [28], the different magnetic moment values of $4\ (N-1)$, $(N-1)$ and $2\ (N-1)\ \mu_B$ were found for bare, singly and doubly H-saturated TGFs, respectively, where N denotes the number of hexagons along each edge of TGFs. This result implies that magnetic moment of TGFs depends on both size and adatom concentration of TGF. The findings indicate that while singly and doubly saturated forms of TGF are possible for H and F atoms, only singly covered and half covered terminations are possible for Li and Be atoms, respectively. On the other hand, stable edge saturated structures of TGFs are not obtained for B, C and N which have larger radii and their interaction with each other do not let them to be placed in a stable configuration. In addition, edge and corner termination of TGFs by single adatom is investigated. Electronic and magnetic properties of singly or doubly covered structures exhibit the same behaviour for several adatom species but single atom termination of these flakes with several adatom species exhibit fairly different properties. Moreover, even corner and edge termination of TGFs by the same single adatom have different effect on the properties of TGFs.

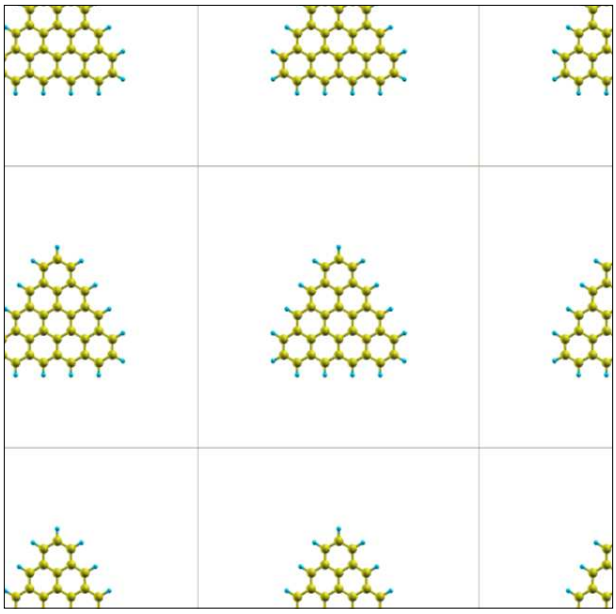

Figure 4.1. TGF in a supercell geometry.

The first principles calculations on electronic structures and geometry optimazitions were performed using the SIESTA package in the frame work of density function theory (DFT). In this chapter we study graphene flakes having equilateral triangular shapes with zigzag edges (TGF). Although we are dealing with single graphene fragment all calculations are performed for periodic systems due to the Bloch theorem can not be

applied to a non-periodic systems. Figure 4.1, shows that in SIESTA calculations, a supercell model was employed such that TGF was put in a large computational box with at least 12Å vacuum space surrounding the TGF that prevents interaction between periodic images of the system.

4.2. Results

In this section, we explore edge functionalization of TGFs in three main subject which they are, bare TGFs, single atom added TGFs and all edge-atom saturated TGFs. All the three cases exhibit quite different geometric, electronic and magnetic properties. This diversity in the properties of the TGFs is crucial for their possible use in future nano electronics.

4.2.1. Bare and Single-Atom-Added TGF

We started edge functionalization investigations with bare flakes. All edge and corner atoms of bare flakes had extra nonbonding electrons. Extra nonbonding electrons of edge and corner atoms exhibited different spin polarizations. H, F, Li, Be, B, C and N atoms were used to manipulate spin polarizations of these edge and corner atoms.

4.2.1.1. Geometric Structure

On the left of Figure 4.2, we present a relaxed geometric structure of the bare zigzag edged triangular graphene flake (*N*-TGF), where *N* denotes the number of edge hexagonal cells in one side of the triangle. On the right of Figure 4.2, red and blue colored carbon atoms denote carbon atoms in A and B sublattice, respectively. As can be seen from the given flake which is 5-TGF, there are 25 (N_A) carbon atoms in A-site and 21 (N_B) carbon atoms in B-site (N_B). Thus there is a relation between the difference of two different site carbon atom number ($N_A - N_B$) and the size of the flake (N), which is $N_A - N_B = N - 1$. This equation will be used in further calculations.

Although, almost entire flake preserve its hexagonal structure, there are some distortions in the carbon-carbon atom bonds which are placed on edge and especially on corner of flake, due to nonbonding electrons of edge and corner C atoms. The bond leghts

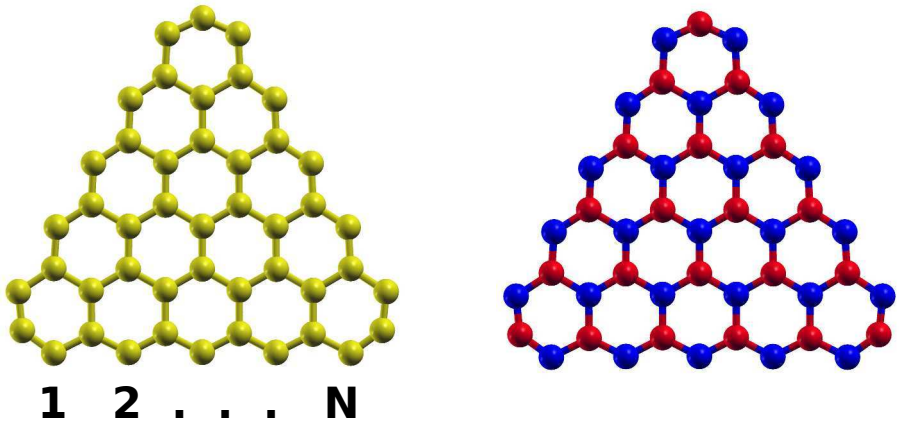

Figure 4.2. Left panel shows the geometric structure of bare N, where N is equal to 5 here. Right panel shows two different site of C atoms in 5-TGF. Red and blue colored C atoms denote C atoms in A and B sublattice.

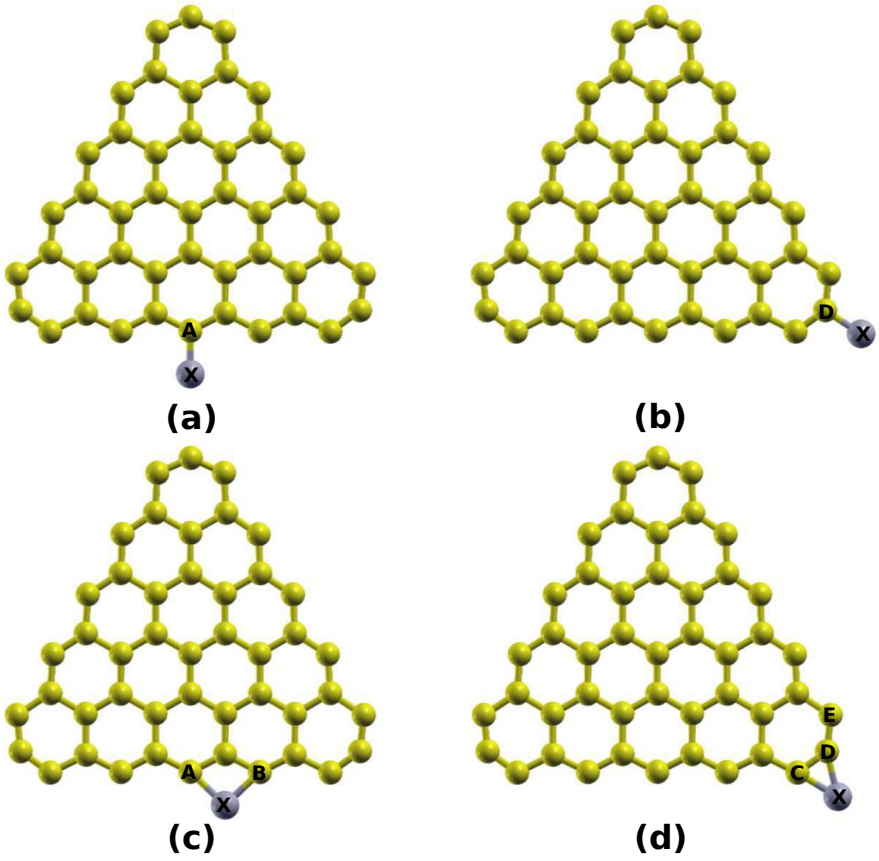

Figure 4.3. Possible binding places for various adatoms (X). Adatoms bonded to (a) edge of TGF and in top site, (b) corner of TGF and in top site, (c) edge of TGF and in bridge site, (d) corner of TGF and in bridge site. Here A, B, C, D and E denote most affected atoms of TGFs from the process of adatom binding.

are 1.42Å near the center of the flake which it reduce to 1.38Å and 1.29Å near the edge and corner of the flake, respectively.

Then, the effect of edge and corner termination of TGFs with a single adatom is investigated. Figure 4.3 shows possible edge and corner binding places for a single adatom. In this section, H, F, Li, Be, B, C and N atoms are used as an adatom. In Figure 4.3, X atom denotes added atoms to the TGF. A, B, C, D, E atoms are the most affected flake atoms from this process. There are two different site of adatoms for bind to the TGF: *top* and *bridge*. As seen from Figure 4.3, in *top* site adatom bind with only one C atom whereas in *bridge* site adatom bind with two C atoms.

Table 4.1 presents bond lenghts and binding energies of single-adatom-added TGFs where these adatoms are placed in edge or corner of TGFs. Binding energies are defined as;

$$E_B = |E_{tot} - E_{bareTGF} - E_{adatom}|. \tag{4.1}$$

Table 4.1 shows that H and F atoms prefer to bind in top site, while other atoms prefer to bind in bridge site of the TGF. As can be seen from the table, when B and C atoms bind to the edge or corner of TGFs, they have the highest binding energies whereas Li and Be atoms have the least binding energies. On the other hand, the same table shows that H atoms have the lowest bond lenghts whereas Li atoms have the longest bond lenghts. Thus, it is hard to find a regular trend for these properties in the table.

Table 4.1. Bond lenghts and binding energies of single-atom-added TGFs.

	Places	**Bond Lenghts (Å)**		**Binding Energies (eV)**	
		Edge	**Corner**	**Edge**	**Corner**
H	Top	1.09	1.10	5.23	3.96
F	Top	1.33	1.33	6.55	5.08
Li	Bridge	2.01	2.02	2.25	0.98
Be	Bridge	1.71	1.66	3.80	1.65
B	Bridge	1.59	1.46	7.69	6.90
C	Bridge	1.47	1.38	7.64	7.73
N	Bridge	1.48	1.39	5.93	5.52

4.2.1.2. Electronic Structure

Pristine graphene has continuous band structure with zero band gap. When graphene is reduced to graphene nano flake (GNF), this flakes have discrete, moleculer energy levels, so the energy of the highest occupied molecular orbital takes the place of the Fermi Energy (E_f). The difference in the energies of the Highest Occupied Molecular Orbital (HOMO) and Lowest Unoccupied Molecular Orbital (LUMO) corresponds to the energy gap (E_g). Figure 4.4 shows electronic energy diagrams of some GNFs. As seen in the Figure, the electronic energy levels in these systems significantly depends on the shape.

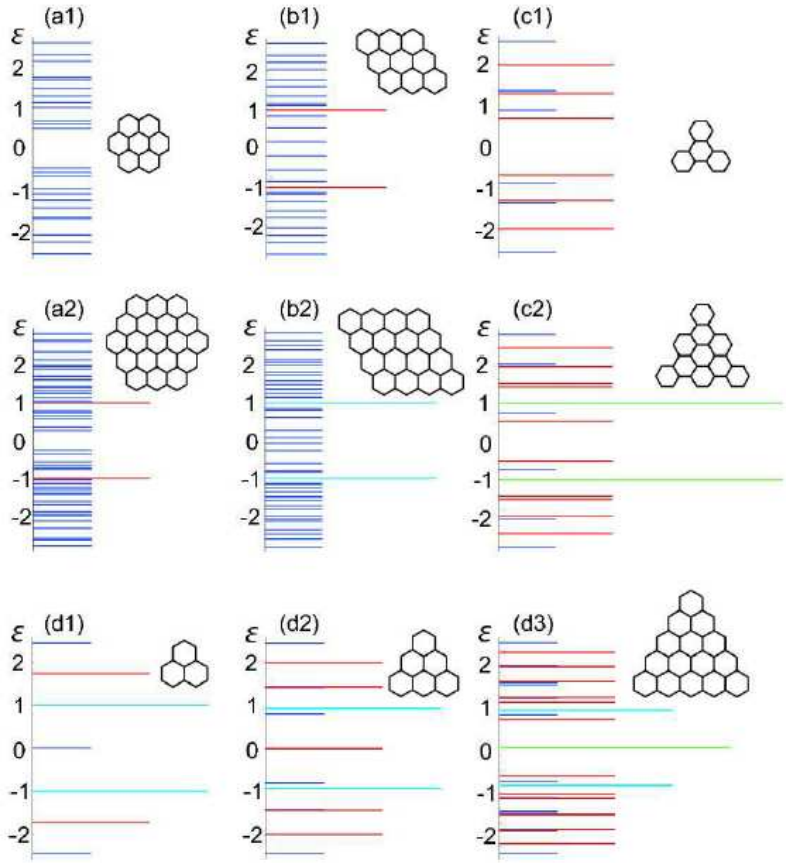

Figure 4.4. Density of states for typical zigzag nanodisks, The horizontal axis is degenarcy and the vertical axis is the energy ε in units of t = 3eV. (a) Hexagonal zigzag nanodisks. (b) Parallelogrammic zigzag nanodisks. (c) Trigonal armchair nanodisks. (d) Trigonal zigzag nanodisks. There are degenerated zero-energy states in all trigonal nanodisks, and they are metallic. There are no zero-energy states in all nanodisks, and they are semiconducting. Adapted from Ref. [70].

Figure 4.5 shows the energy spectra of a bare 5-TGF. We determined the spin polarized states for this bare flake in the vicinity of fermi level. Each inner C atom of bare

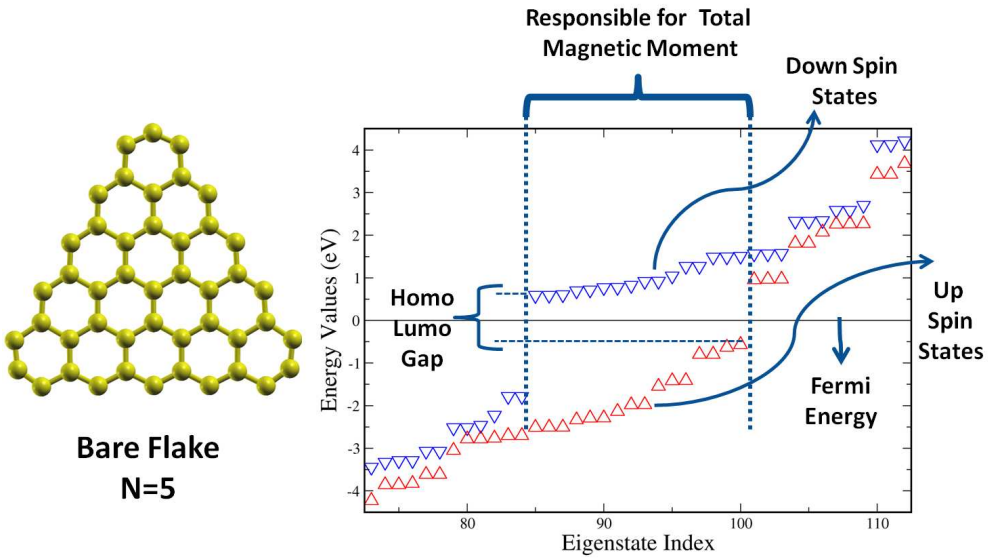

Figure 4.5. Left of the figure illustrate the zigzag edged bare TGF and right of the figure shows the energy values of electrons of that TGF which belong up spin states and down spin states near the fermi energy. Fermi energy shifted to 0.

TGF is connected with the three nearest neighbors while leaving behind a one p_z orbital electron. These electrons in each sublattice have opposite spin state and make spin paired π bonds, thereby all inner C atoms of flake are spin non-polarized. Thus, spin polarized states near the fermi level, which are shown in Figure 4.5, belong to edge C atoms and there is no spin degeneracy for inner atom states. Edge C atoms of bare flakes that make only two bonds contribute to the spin polarized states with two nonbonding electrons. As a result, the Lieb's theorem as applied to a bare N-TGF can be modified as such $3N$ edge atoms of sublattice A, and 3 corner atoms of sublattice B should be counted twice. Therefore the number of spin non-degenerate states (N_S) in a N-TGF becomes:

$$N_S = N - 1 + 3N - 3 = 4N - 4. \tag{4.2}$$

N_S related to its magnetic moment simply defined as $\mu = N_S\ \mu_B$. The effect of single adatom termination with several elements (H, F, Li, Be, B, C and N) on the electronic properties of 5-TGF is investigated. Figures 4.6 and 4.7 show that energy spectrum of these TGFs is closely dependent on the type and binding site of adatom. Addition of a single atom to a TGF introduces additional states around the fermi level. The number of these additional states depends on valance electron number of the adatom. As seen in

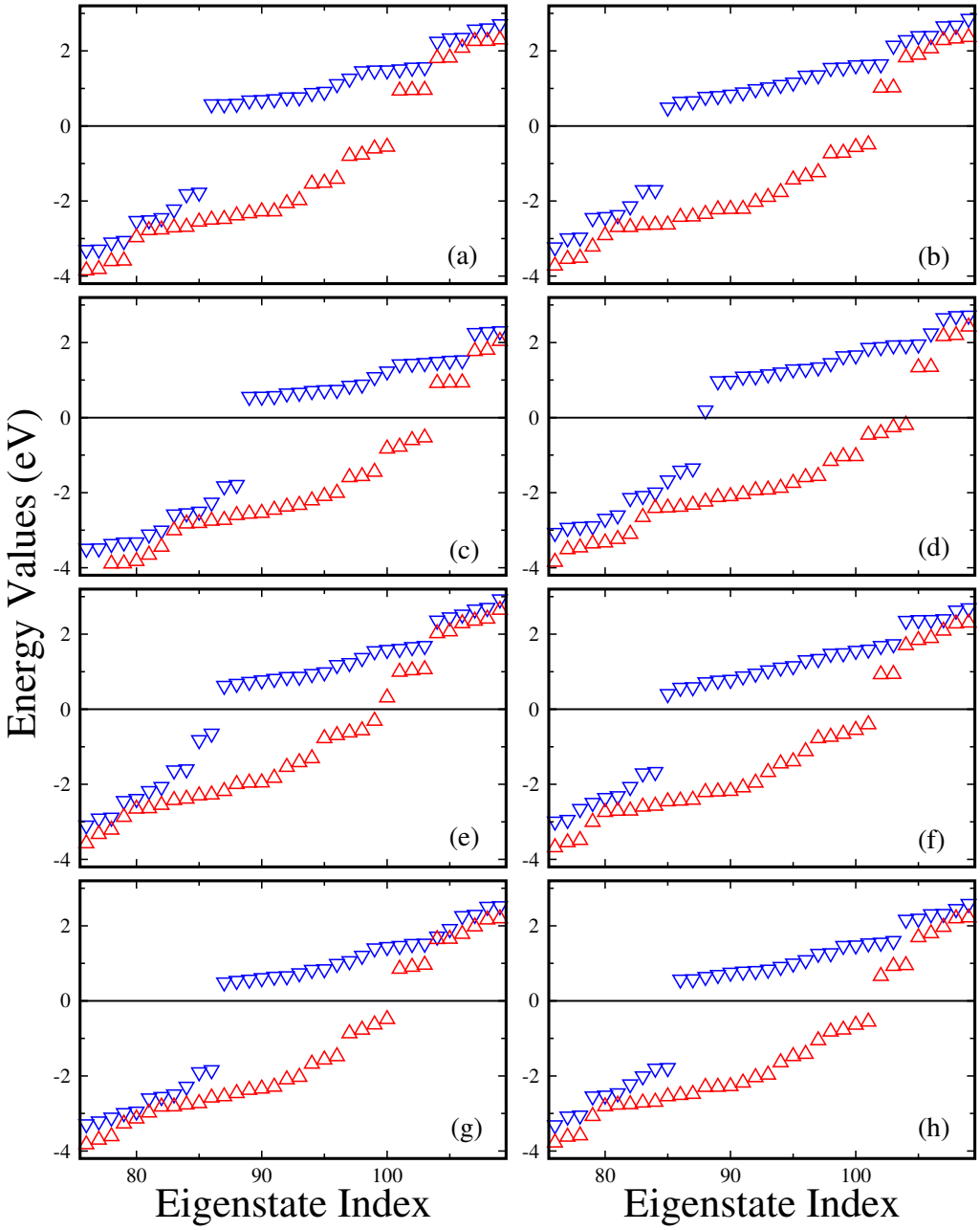

Figure 4.6. Energy spectra of 5-TGF with a single-adatom. (a) H atom bonded to edge, (b) H atom bonded to corner, (c) F atom bonded to edge, (d) F atom bonded to corner, (e) Li atom bonded to edge, (f) Li atom bonded to corner, (g) Be atom bonded to edge, (h) Be atom bonded to corner.

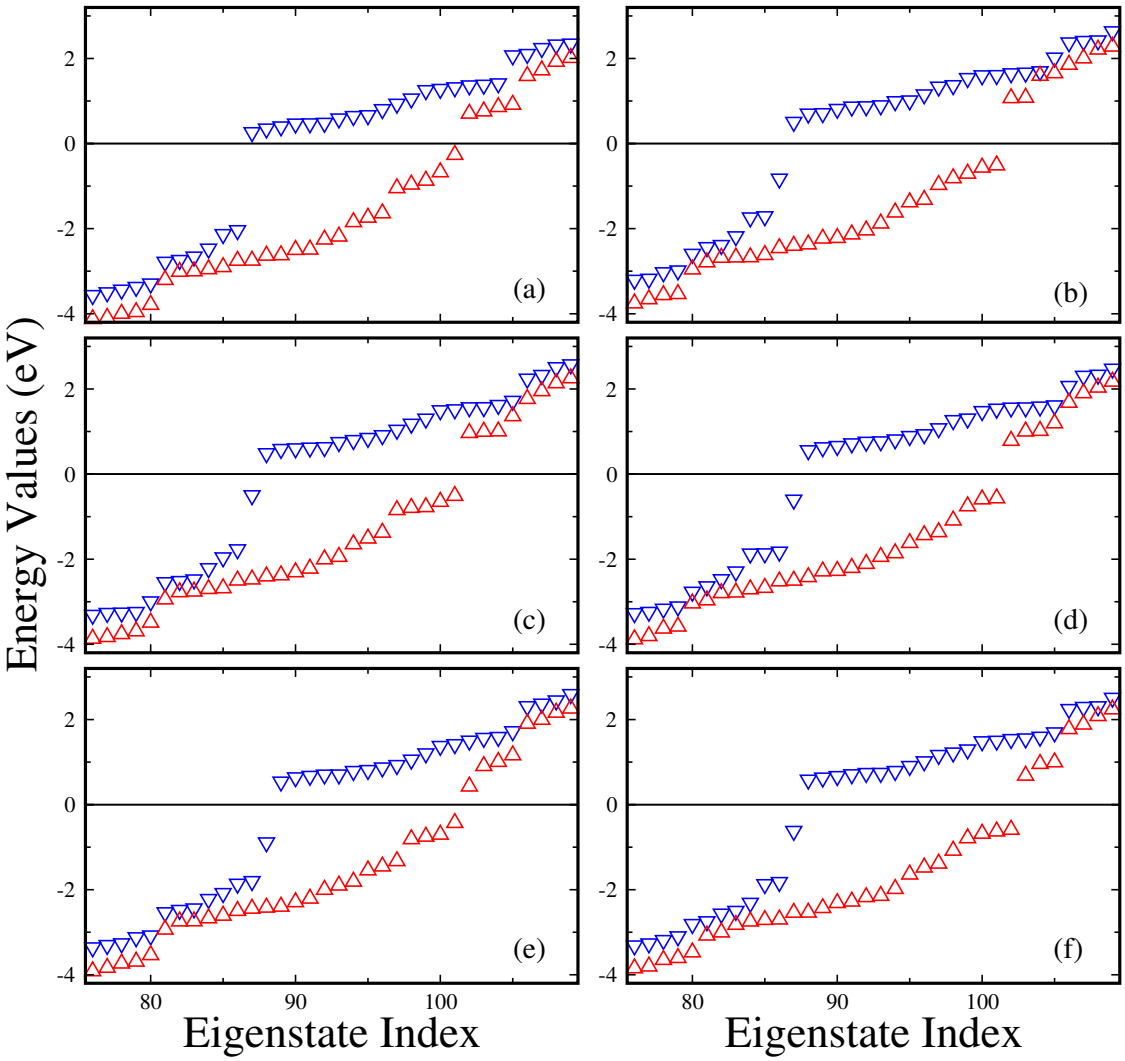

Figure 4.7. Energy spectra of 5-TGF with a single-adatom. (a) B atom bonded to edge, (b) B atom bonded to corner, (c) C atom bonded to edge, (d) C atom bonded to corner, (e) N atom bonded to edge, (f) N atom bonded to corner.

Figures 4.6 and 4.7 this process removes the spin polarized states related to the dangling bonds and change the value of N_S.

H, F, Li, Be, B, C and N adatoms have 1, 7, 1, 2, 3, 4 and 5 valance electrons, respectively. As expected, Figures 4.6 (a) and (b) show that, if H atoms binded to the edge of TGF, one polarized majority spin state becomes spin un-polarized whereas the same atom binded to corner of TGF one polarized minority spin state becomes spin un-polarized. Thus, although the same atoms are added to flake, their contribution to the N_S is different and it deeply depends on the binding position of adatoms.

Single F atom added case is shown in Figures 4.6 (c) and (d). Even though F atom has 7 valance electrons, it exhibits almost the same electronic structure with H atom added case. Figure 4.6 (e) illustrates that the effect on the electronic properties of corner

termination of TGFs with Li and H adatoms are almost the same. But edge termination of TGF with Li atom is more complicated. Energy spectra of the edge terminated TGFs with H and Li atoms (figures 4.6 (a) and (e) respectively), are fairly different although Li and H atoms have the same valence. When Li atom binded to the edge atoms of TGF one polarized majority spin state becomes spin un-polarized and another polarized majority spin state turns into a minority spin state. As a result edge termination of TGF with Li element reduce N_S by three. On the other hand, there is no noticeable difference between the energy spectra of edge and the corner termination of TGFs by Be, B and C atoms.

Addition of Be, B, C, and N atoms to the edge of TGF remove 2, 2, 3, and 4 polarized majority spin state, respectively, and B, C, N atoms contribute one new polarized majority spin state. Thus edge termination with Be, B, C, and N atoms reduce N_S by 2, 1, 2, 3. On the other hand, corner termination with Be, B, C, and N atoms remove 1, 2, 3, and 3 polarized majority spin state, respectively, and Be, B, C atoms contribute one polarized majority spin state whereas N atom contribute two. As a result, when Be, B, C, and N atoms bind to corner of TGF, Be addition does not affect N_S whereas B, C, and N addition reduce N_S by 1, 2, 1, respectively.

4.2.1.3. Magnetic Structure

In this part, the effect of termination by single atom on the magnetization of bare TGF is investigated. H, F, Li, Be, B, C and N atoms are used as adatoms in this part. Figure 4.8 (a) displays the spin dependent charge densities of a bare TGF. It is clear that, three corner atoms have minority spin component whereas all edge atoms have majority spin component with ferromagnetic ordering. Single atom can be put in two different binding sites on the sides of TGF, which are called as edge and corner termination. These two different binding types, lead to different effects on the magnetic structure of the flake. As shown in Figures 4.8 and 4.9, not only binding site but also adatom species have significant effect on the net magnetic moment of TGF. In Figures 4.8 and 4.9, the given symbols and numbers are symbols of adatom and net magnetic moments of single atom added TGFs which are in given units of μ_B. On the other hand, binding geometries of adatoms have also a significant effect on the magnetic properties of TGFs. As seen in Figures 4.8 and 4.9, an adatom binding at a top site reduces magnetic moment of only one edge-C atoms while an adatom bind at a bridge site reduces magnetic moment of two edge-C atoms.

Total valance charges and net magnetic moments of some flake atoms, adatoms

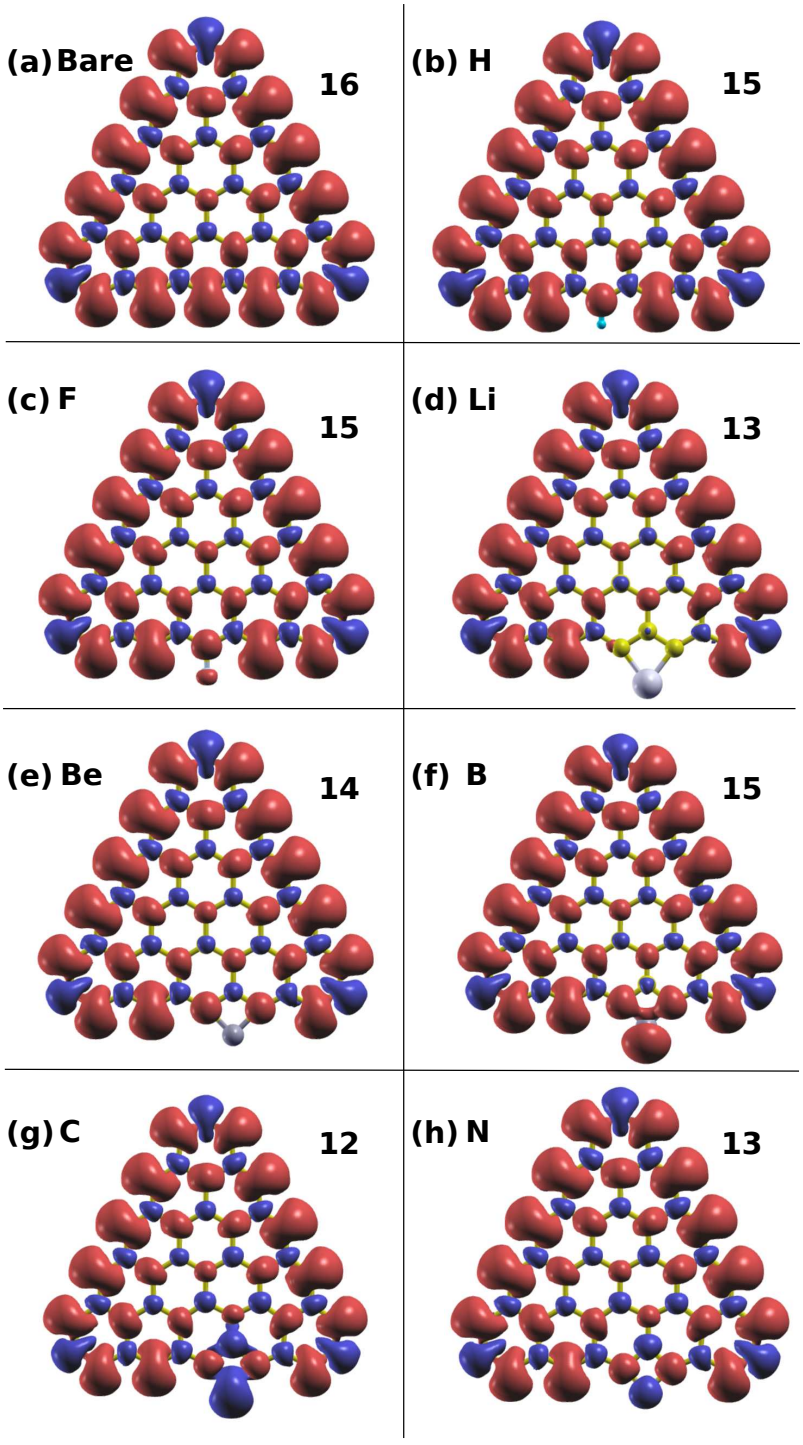

Figure 4.8. Isosurfaces of charge density difference of spin-up (↑) and spin-down (↓) states for 5-TGF; bare (a), and single adatom H, F, Li, Be, B, C, N (b)-(h) terminated at edge of flakes respectively.

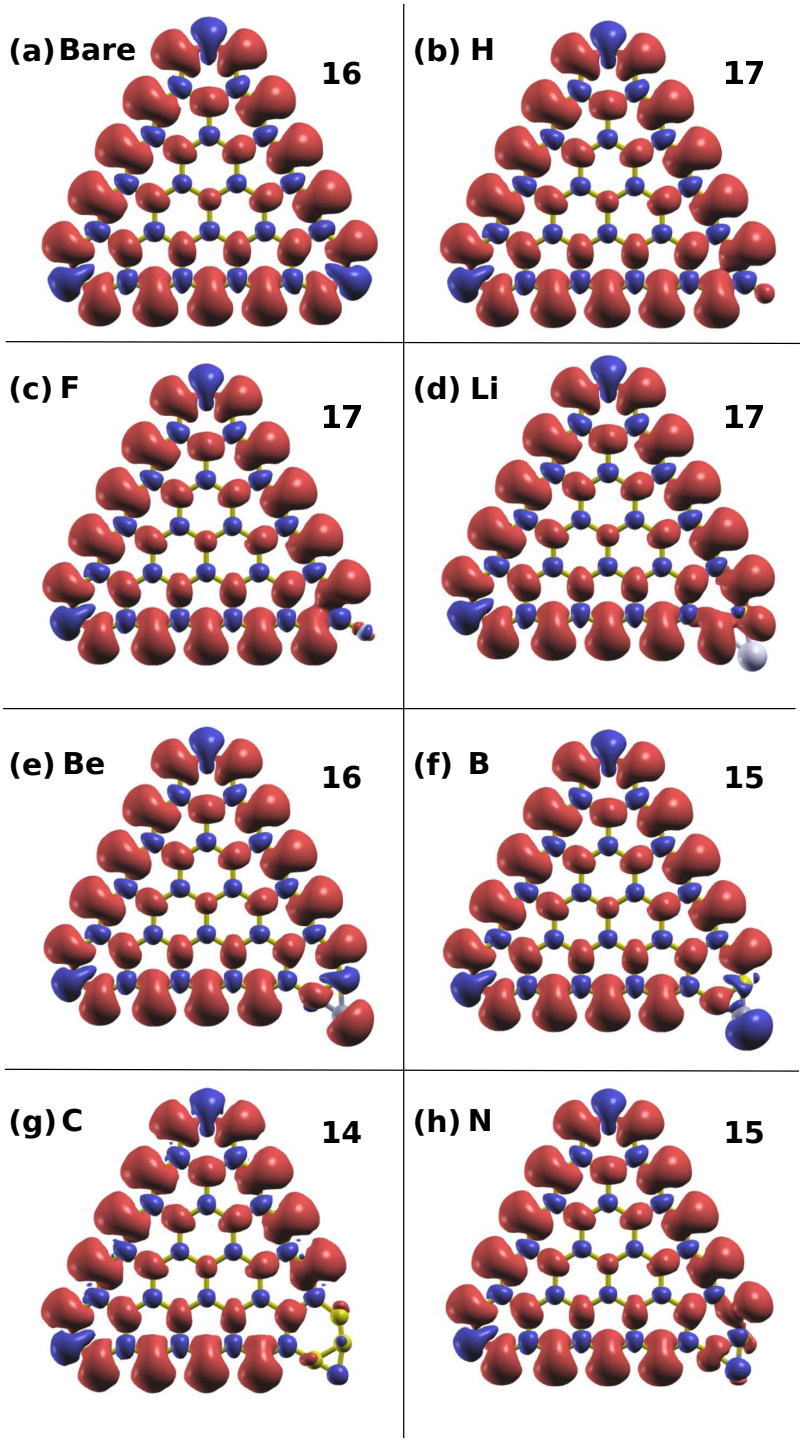

Figure 4.9. Isosurfaces of charge density difference of spin-up (↑) and spin-down (↓) states for 5-TGF; bare (a), and single adatom H, F, Li, Be, B, C, N (b)-(h) terminated at corner of flakes respectively.

and whole flake are given in Table 4.2. As seen in Figure 4.8 (a), due to imblance in the atom number of different sublattices and presence of unsaturated edge atoms, there is considerable moment accumulation on the edge carbon atoms of bare TGF. According to the Mulliken population analysis, avarage magnetic moment of edge atoms of bare TGF is $1.22\ \mu_B$, and it reduces to 0.90 μ_B for the nearest-neighbors of the corner atoms whereas corner atoms' avarage magnetic moment is $-0.38\ \mu_B$ and the spins of these atoms are in the opposite direction to the spins of edge carbon atoms (see Table 4.2). As a result, the total net magnetic moment of bare 5-TGF is $16\ \mu_B$, and this result is in accordance with the Lieb's theorem.

Figures 4.8 (b), (c) and 4.9 (b), (c) show that although H and F atoms have different number of electrons, single H and F added TGFs exhibit similar magnetic properties. The spin polarization of the edge and corner C atom of TGF considerably decreases as the H or F atoms bind in a top site to these atoms. When H or F atoms bind to the edge C atom of TGF, which these edge atoms have majority spin component, the net magnetic moment of bare TGF decrease by 1 μ_B. If they bind to a corner C atom of TGF, which these corner atoms have minority spin component, the net magnetic moment of bare TGF increase by $1\mu_B$. Thus, edge and corner saturated TGFs by single H or F atoms, have 15 and 17 μ_B total net magnetic moments, respectively. As seen in Table 4.2, there are almost no net induced magnetic moments on the H and F atoms. Furthermore, same Table shows that when H atoms bind to edge or corner of TGF, they gain extra charge from TGF whereas F atoms' charge transfer is insignificant.

Due to preference of Li, Be, B, C and N atoms to bind at the bridge site of two edge or corner C atoms, understanding the effect of functionalization on the TGF by these atoms is quite complicated. Thus to find the ground state, several initial spin configurations of flake and added atoms are tried and the lowest energy configurations are depicted in Figures 4.8 and 4.9.

Table 4.2 shows that when a Li atom is placed at an edge of TGF, edge C atoms become non-magnetic, however when Be, B, C or N atoms are placed at an edge of TGF, edge C atoms lose approximately 75% of their magnetic moments. Figures 4.8 (d)-(h) illustrate that Li and Be atoms are almost non-magnetic, B atoms have same spin polarization, C and N atoms have opposite spin polarization with the edge-C atoms, and their net magnetic moment values are 0.86, -1.3 and -0.47 μ_B, respectively. Table 4.2 also shows that B atom gains extra approximately 17% charge from edge atoms of flake whereas there is not noticeable charge transfer for other adatoms.

When single adatom bind to corner of TGF in *bridge* site, one adatom makes two

Table 4.2. Charge and magnetic moment values of some flake atoms, added atom and all flake. X denotes adatoms.

		Total Charge		**Magnetic moment (μB)**		
	Symbol of Flake atoms	**Flake atoms**	**X**	**Flake atoms**	**X**	**All flake**
Bare flake	A, B, C D, E	4.05, 4.05, 4.06 3.98, 4.06	-	1.23, 1.21, 0.90 -0.38, 0.90	-	16
H on edge	A	3.78	1.25	0.32	0.0	15
H on corner	C, D, E	4.02, 3.74, 4.03	1.24	1.20, -0.11, 1.21	0.04	17
F on edge	A	4.08	6.90	0.29	0.04	15
F on corner	C, D, E	4.04, 4.06, 4.04	6.90	1.20, -0.06, 1.20	0.0	17
Li on edge	A, B	4.15, 4.15	0.92	0.01, 0.0	0.01	13
Li on corner	C, D, E	4.10, 4.14, 4.04	0.71	0.74, 0.26, 1.13	0.17	17
Be on edge	A, B	4.09, 4.09	1.93	0.32, 0.30	-0.03	14
Be on corner	C, D, E	4.05, 4.07, 3.98	2.00	0.20, -0.18, 0.88	0.52	16
B on edge	A, B	3.84, 3.84	3.50	0.36, 0.35	0.86	15
B on corner	C, D, E	3.70, 3.73, 4.08	3.64	0.20, -0.04, 0.89	-0.63	15
C on edge	A, B	4.03, 4.03	4.10	0.39, 0.38	-1.3	14
C on corner	C, D, E	3.92, 3.99, 4.06	4.10	0.04, -0.03, 0.02	-0.09	14
N on edge	A, B	4.10, 4.07	4.91	0.29, 0.33	-0.47	13
N on corner	C, D, E	4.11, 4.08, 4.13	4.76	0.18, -0.05, 0.85	-0.15	15

bonds, one of them with an edge C atom and the other with a corner C atom of TGF. Figure 4.9 (d) shows that when Li atom bind to corner of TGF, spin states of corner atom of TGF is flip. When Be, B and N atoms are placed at corner of TGF, magnetic moments of attached edge and corner atoms of flake decrease. Furthermore, in the corner termination of TGF by a C atom, one corner and its two neighboring edge atoms become non-magnetic. Table 4.2 shows that B, C and N atoms have minority spin component whereas Be has majority spin component, with net magnetic values of -0.63, -0.09, -0.15 and 0.52, respectively.

As seen in Figures 4.8 and 4.9, while the nature of edge or corner saturation by H or F is well understood, edge functionalization with other adatoms shows irregular trends. For example, although Li atom has less valence charge, it reduces total magnetic moment of flake, by 3 when bond to an edge of TGF, however when it is bond to a corner of TGF it increases total magnetic moment by 1 μ_B. As a result, there is not a simple explanation for edge or corner termination of TGF by Li, Be, B, C and N atoms. To have a deeper insight about the edge functionalization of TGF we will examine the magnetic properties of half, full and doubly saturated structures of TGFs.

4.2.2. Saturating All Edge-Atoms of TGF

To conclude, edge functionalization of TGFs, saturation of all edge atoms of TGFs are analyzed in this part. These structures are more stable than bare and single-atom-added TGFs due to saturation of all dangling bonds of the flake.

4.2.2.1. Geometric Structure

Saturating all edge-atoms of TGFs are more stable relative to bare or single-atom-added TGFs. Three different concentrations of adatoms for saturation of edges are considered which are, half-covarage (HC-X) where adatoms are bound to every other bridge site only, full-covarage (FC-X) where there is one adatom for each edge atom, and double-covarage (DC-X) where there are two adatoms for each edge atom. Here X denotes the type of the adatoms. In our calculations we found that, HC, FC and DC structures terminated with B, C and N atoms are not stable. When these atoms are placed around the TGF, the interaction between them cause some distortions on the honeycomb structure of TGF and geometry optimizations for these adatom types can not be handled.

Figures 4.10 (a) and (c) show geometric structures of FC-H and FC-F cases. In these configurations all the edge atoms make sp^2 hybridization like inner C atoms. Since dangling bonds of all edge atoms are saturated with adatoms, these structures are considerably more stable than bare and single-atom-added TGFs. In FC-H and FC-F cases with size N=5, the avaraged C-C bond leghts are approximately 1.42, 1.40 and 1.39Å near the center, edge and corner of the flakes, respectively. Table 4.3 shows that binding energies of H and F atoms are fairly large, C-H and C-F bond lenghts are small relative to the other atoms and H and F atoms bind to only one edge or corner atom of TGF in a top site. Thus geometry optimizations of FC-H and FC-F cases are relatively easy. Moreover DC-H and DC-F cases are also possible for H and F atoms. Figures 4.10 (b) and (d) present optimized geometric structures of DC-H and DC-F cases, respectively. Apart from other configurations, in these structures edge or corner atoms of flake have sp^3 hybridized electrons. Each edge and corner carbon atom is bonding with 2 adatoms. These adatoms are located out of plane in opposite directions. Table 4.3 shows that binding energies of DC-H and DC-F cases are half of the FC-H and FC-F cases, respectively. The Same table shows that, in DC-F case, z-distances are larger relative to DC-H case, due to larger size F atoms. In DC-H and DC-F cases with *N*=5, the avarage C-C bond leght is 1.42Å near

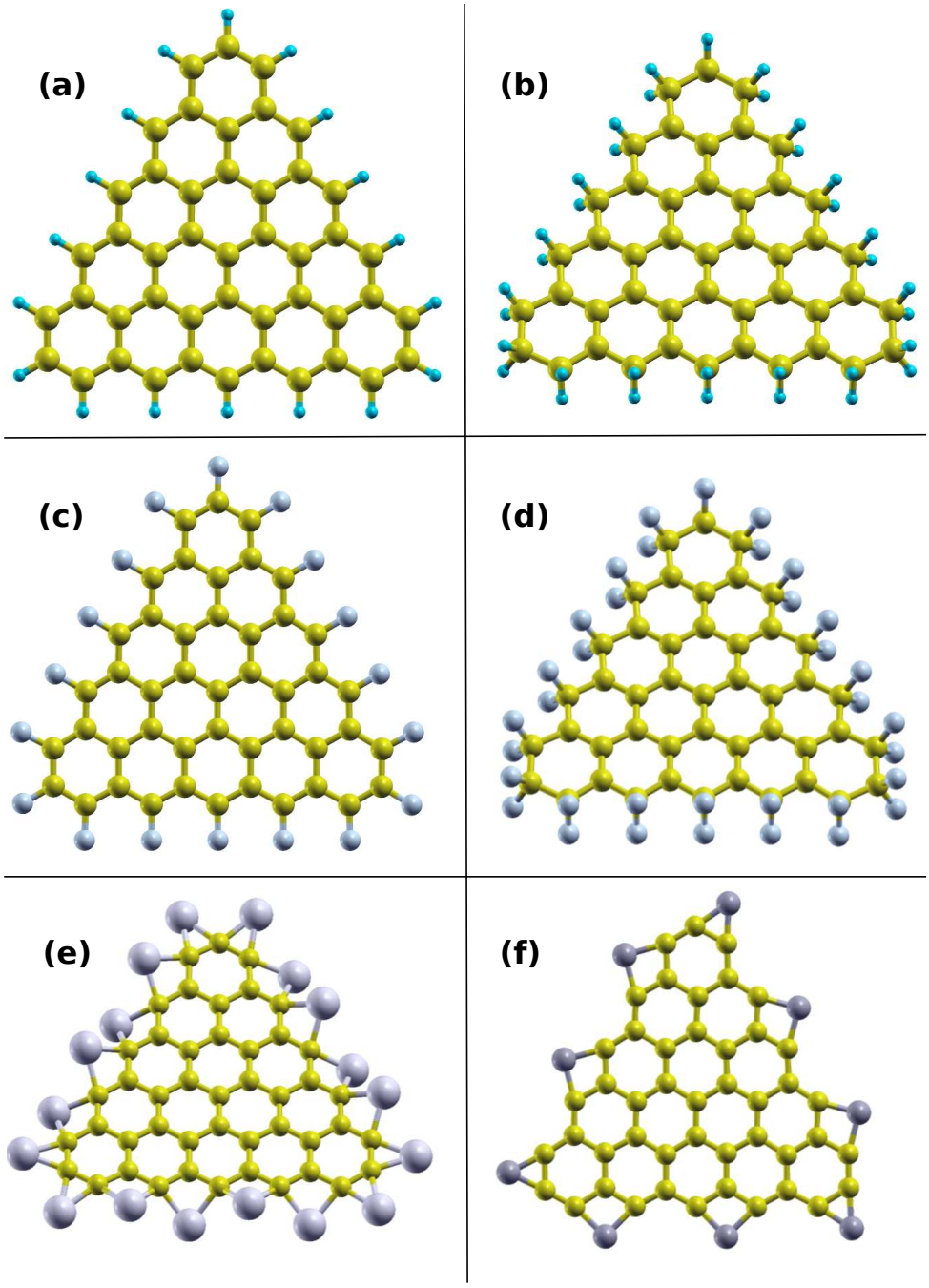

Figure 4.10. Optimized geometric structures of all-edge-atoms-saturated TGFs: (a) 5-FC-H, (b) 5-DC-H, (c) 5-FC-F, (d) 5-DC-F, (e) 5-FC-Li and (f) 5-HC-Be.

the center of the flake, which increases to 1.47Å and 1.53Å near the edge and corner of the flake, respectively. As a result, addition of H and F to TGF, make strain at the edge and corner of TGF.

Table 4.3. Bond lenghts and binding energies of all-edge-atoms-saturated TGFs.

	Places	**Bond Lenghts (Å)**	**Z-Distances (Å)**	Binding Energies (eV)
5-FC-H	Top	1.09	-	5.01
5-FC-F	Top	1.33	-	6.27
5-FC-Li	Bridge	1.99	0.51	1.53
5-HC-Be	Bridge	1.69	-	2.92
5-DC-H	Top	1.11	0.77	2.5
5-DC-F	Top	1.37	1.02	3.14

The binding energy per adatom is calculated by;

$$E_B = |E_{tot} - E_{bareTGF} - (n.E_{adatom})|/n, \tag{4.3}$$

where E_{tot} is the energy of final structure, $E_{bareTGF}$ is the total energy of bare TGF and E_{adatom} is the energy of single adatom.

We have mentioned before that, Li and Be atoms bind to two edge or corner atoms of TGF in bridge site. Table 4.3 reveals that, C-Li and C-Be bond lenghts are quite large compare to other bond lenghts. Relaxed geometric structure of FC-Li case is shown in Figure 4.10 (e). As can be seen from this figure, because of long bond lenghts, two neighbouring Li atoms move away from eachother and they placed in opposite directions relative to the plane of TGF. Avarage C-Li bond lenghts and z-distances are given in Table 4.3. In this structure each edge and corner atom binds with two different Li atoms and avarage C-C bond lenghts are 1.42Å near the center and edge of TGF whereas 1.40Å near the corner of TGF. Figure 4.10 (f) shows the geometric structure of HC-Be case. In HC-Be case, due to low concentration, Be atoms prefer to bind edge atoms in the plane of TGF. Apart from FC-Li case, each edge or corner atoms of TGFs bind with only one adatom (Be). Table 4.3 shows that, in HC-Be case, although concentration of Be atoms is low, binding energies of this atoms are quite small. In HC-Be with size *N*=5, avaraged C-C bond lenght is 1.42Å near the center of TGF. C-C bond lenght changes from 1.37 to 1.47Å in the vicinity of the edge and corner of TGF.

4.2.2.2. Electronic Structure

In previous sections, it was shown that the electronic energy levels in TGFs crucially depend on the type and the binding site of the single adatom. To understand more clearly the effect of edge functionalization on the electronic properties of TGFs, all-edge-atoms saturated TGFs were investigated. Energy spectra of bare, FC-H, FC-F, DC-H, DC-F, FC-Li and HC-BE are shown in Figures 4.11 and 4.12 for N=5 and N=6. It was

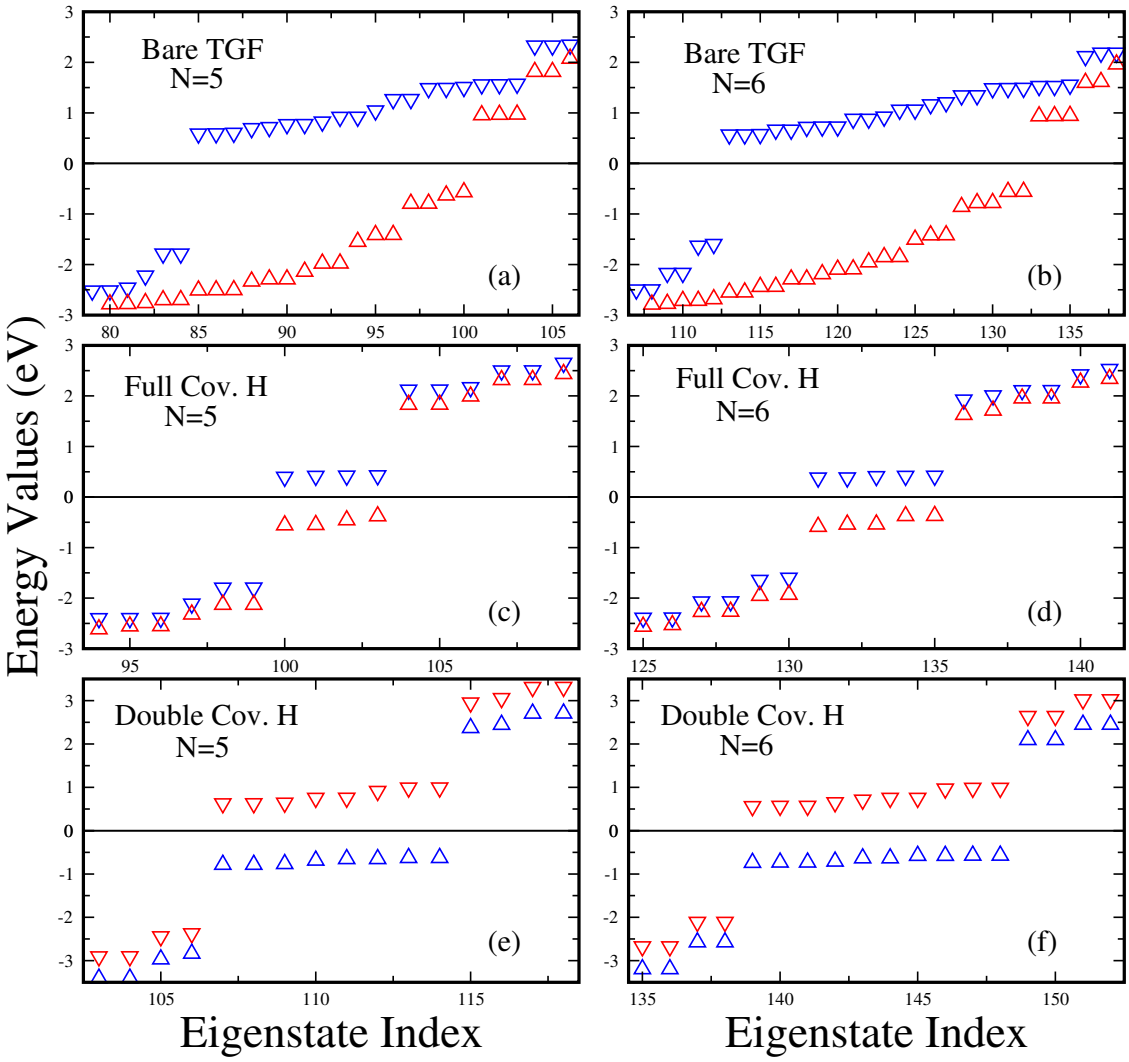

Figure 4.11. Energy spectra of (a) bare 5-TGF, (b) bare 6-TGF, (c) 5-FC-H, (d) 6-FC-H, (e) 5-DC-H, (f) 6-DC-H.

found that in previous parts, in bare flake there was a relation between the size of flake (N) and the number of spin non-degenerate states (N_S) as $N_s = 4N-4$. This equality is consistent with Figures 4.11 (a), (b). In FC case, where all the C atoms make sp^2 hybridization and dangling bonds contribution of edge atoms to the N_S were vanishing. All

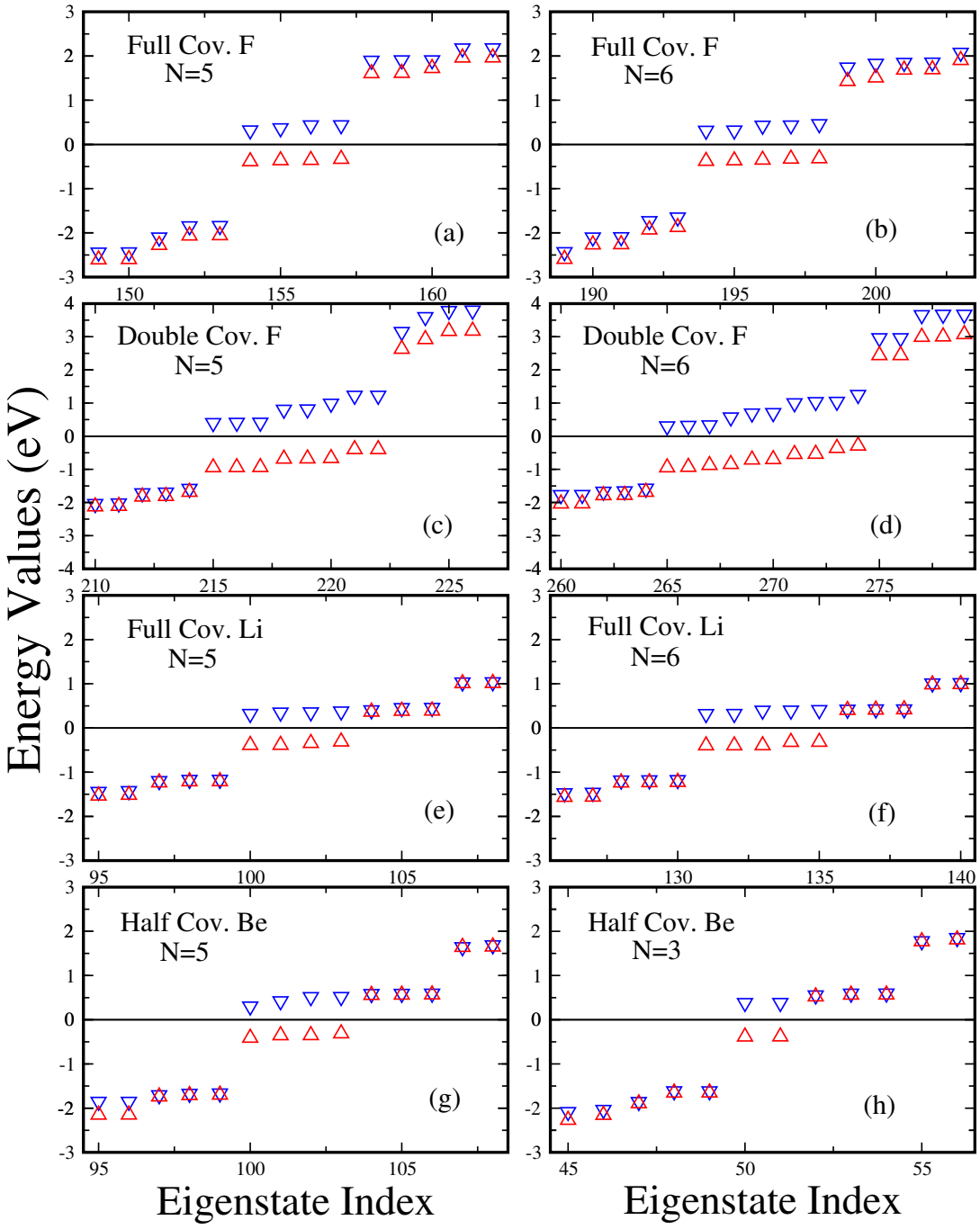

Figure 4.12. Energy spectra of (c) 5-FC-F, (d) 6-FC-F, (e) 5-DC-F, (f) 6-DC-F, (e) 5-FC-Li, (f) 6-FC-Li, (g) 5-HC-Be (h) 3-HC-Be.

contribution to the N_S comes from nonbonding P_z orbitals. Due to contribution of the C atoms of different sublattices cancel each other, difference in the numbers of atoms of different sublattice contribute to N_S. As a result in FC cases $N_S = N_A - N_B = N-1$ in accordance with Lieb's theorem. This result is consistent with Figures 4.11 (c), (d). Lastly, in DC cases (Figures 4.11 (e), (f)), all edge atoms make sp^3 hybridization. Edge atoms' contribution to the N_s disappears. Thus, in this case $N_S = |N - 1 - 3N + 3| = 2(N - 1)$, but here this contribution comes from the minority spin component.

Tunability of the N_s value of TGFs through degree of hydrogenation is an interesting feature. Moreover the effect of edge termination of TGF by F, Li and Be atom, on the electronic properties of TGFs are also discussed in this section. Figures 4.12 (a) and (b) show energy spectra of FC-F and DC-F, respectively. Figures 4.11 (c)-(d) and 4.12 (a)-(d) illustrate that, in the vicinity of fermi level, energy spectra of FC-H and DC-H cases exhibit similiar behaviour with FC-F and DC-F, respectively. Electronic properties of the FC-Li cases with $N = 5, 6$ are investigated and energy spectra is shown in Figures 4.12 (e), (f). As seen in these figures, since Li atoms more metallic than other adatoms, electron energy states of FC-Li case are quite close to the fermi level. On the other hand, energy spectra of the HC-Be cases with $N = 5, 3$ are shown in Figures 4.12 (g), (h). These Figures show that, despite adatom concentration of HC-Be case is halved compared to FC structures, energy spectra of HC-Be case exhibit almost same behaivour with FC cases. This phenomenon can be explained with the fact of valence electron number of Be is two whereas Li and H atoms valance electron number just one. Thus, when Be atom bind to edge of TGF, it removes two polarized majority spin states of the binded edge atoms. Valance electron number of F atom also greater one, however it removes only one polarized majority spin state, due to it binds to only one edge atom.

The change of HOMO-LUMO energy gap with respect to the size and edge termination is plotted in Figure 4.13. It is obvious that the HOMO-LUMO gap gets narrower upon the termination with adatom except some sizes of DC-H and DC-F cases. Figure 4.13 shows that DC-H and DC-F cases are more effective than FC-H and FC-F in the tuning the energy gap. Greater than N=3, for all structures except bare flake, HOMO-LUMO gap reduces when the size increases. HOMO-LUMO gap disappear for large N values in the limit of infinite graphene.

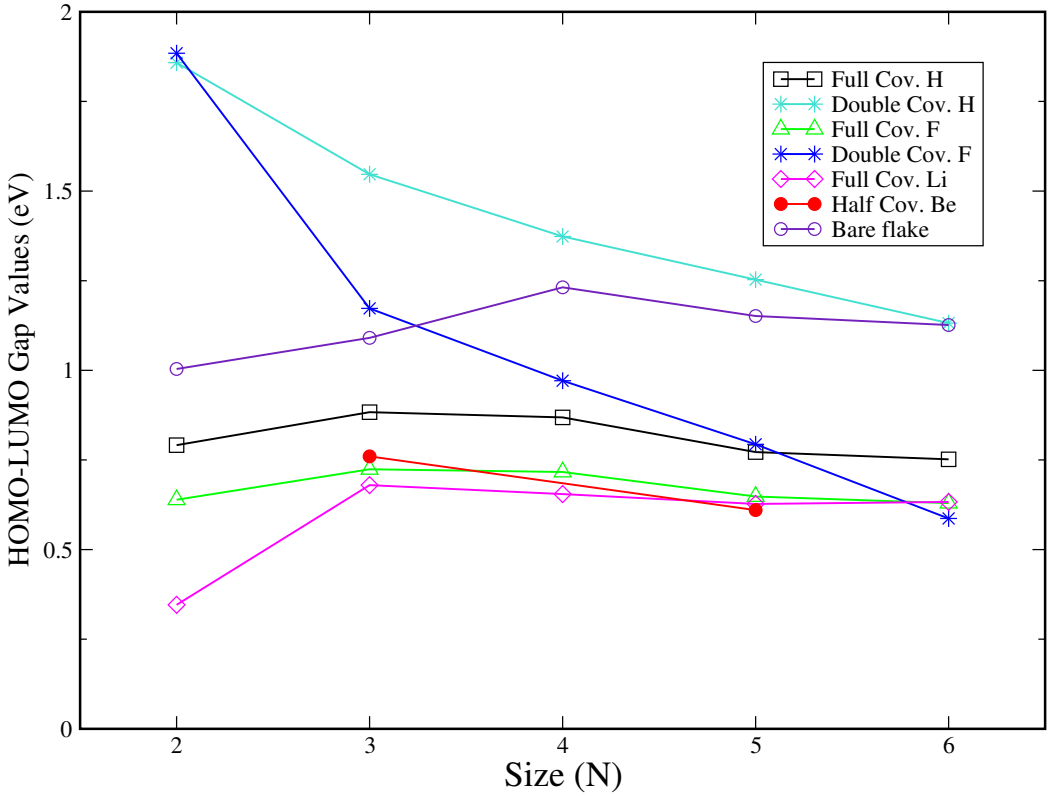

Figure 4.13. Change of HOMO-LUMO gap with respect to size N of the N-TGF with different adatom edge termination.

4.2.2.3. Magnetic Structure

Recent studies have shown that ground state of TGFs is ferromagnetic [25, 27, 63]. The aim of this section is to figure out how this magnetic ground state may be modified by functionalization with adatoms. In this section magnetic properties of FC-H, FC-F, DC-H, DC-F, FC-Li and HC-Be were analyzed. All edge atoms saturated TGFs with B, C and N adatoms were also investigated, however their stable structures did not obtain.

In Figures 4.14 and 4.15, the optimized structures and spin charge density difference isosurface of possible HC, FC, DC cases are presented for two different sizes. Figures 4.14 (a)-(f) and 4.15 (a),(b) show that, FC and DC structures of TGFs with H and F atoms exhibit fairly similar spin localization structures. Thanks to short bond lenght, when H and F atoms bind to edge of TGFs, there was no interaction between the adjacent adatoms. In FC-H and FC-F, magnetic moment of all edge atoms were fairly low compared to edge atoms of bare flakes and all the C atoms have sp^2 hybridized electrons. Table 4.4 gives that, when all edge atoms of bare flake saturated with single H (F) atom avarage magnetic moment of edge atoms decrease from 0.74 to 0.20 (0.17) μ_B and the net

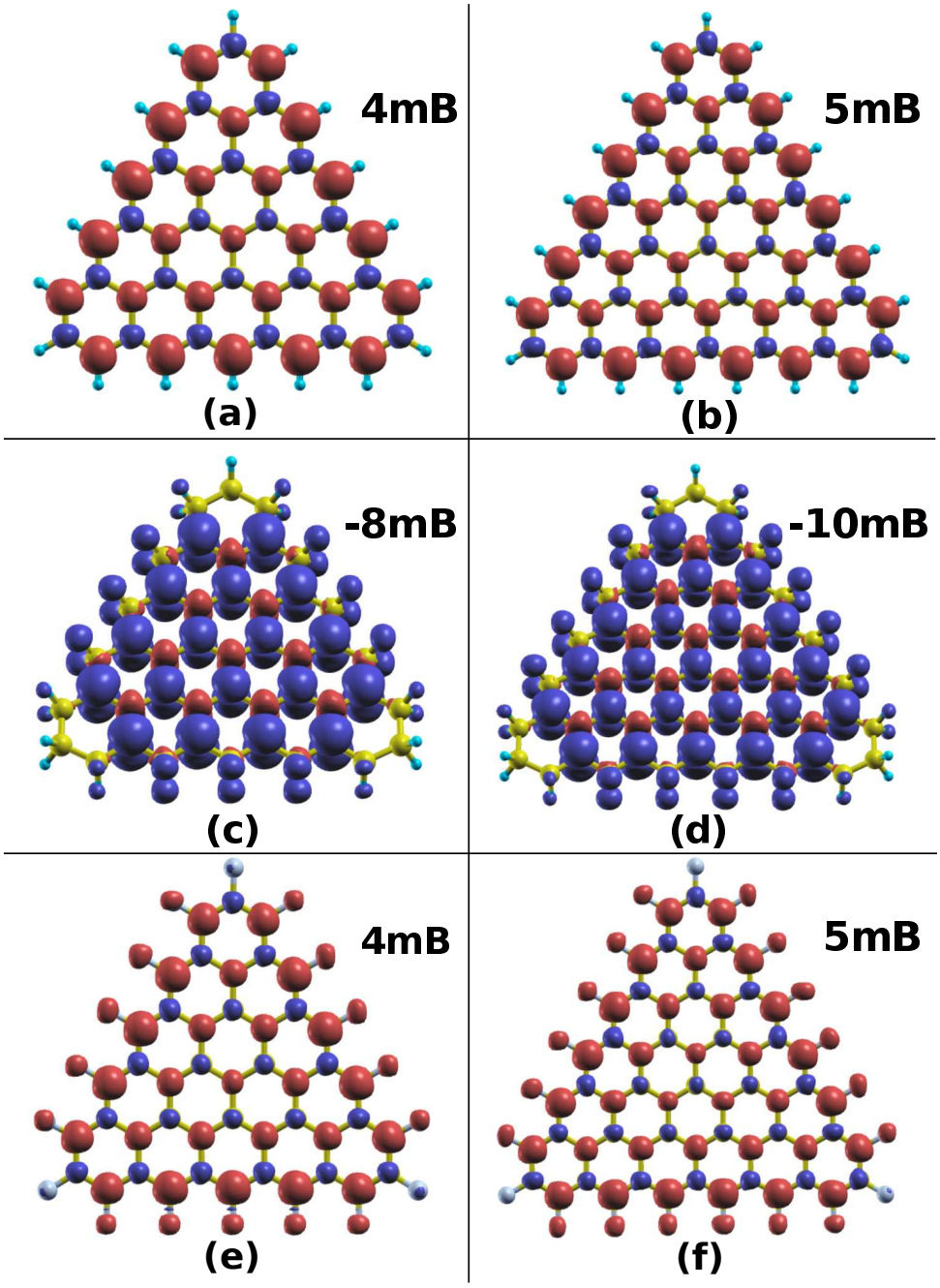

Figure 4.14. Isosurfaces of charge density difference of spin-up (↑) and spin-down (↓) states for all-edge-atoms-saturated TGFs; (a) 5-FC-H, (b) 6-FC-H, (c) 5-DC-H, (d) 6-DC-H, (e) 5-FC-F, (f) 6-FC-F.

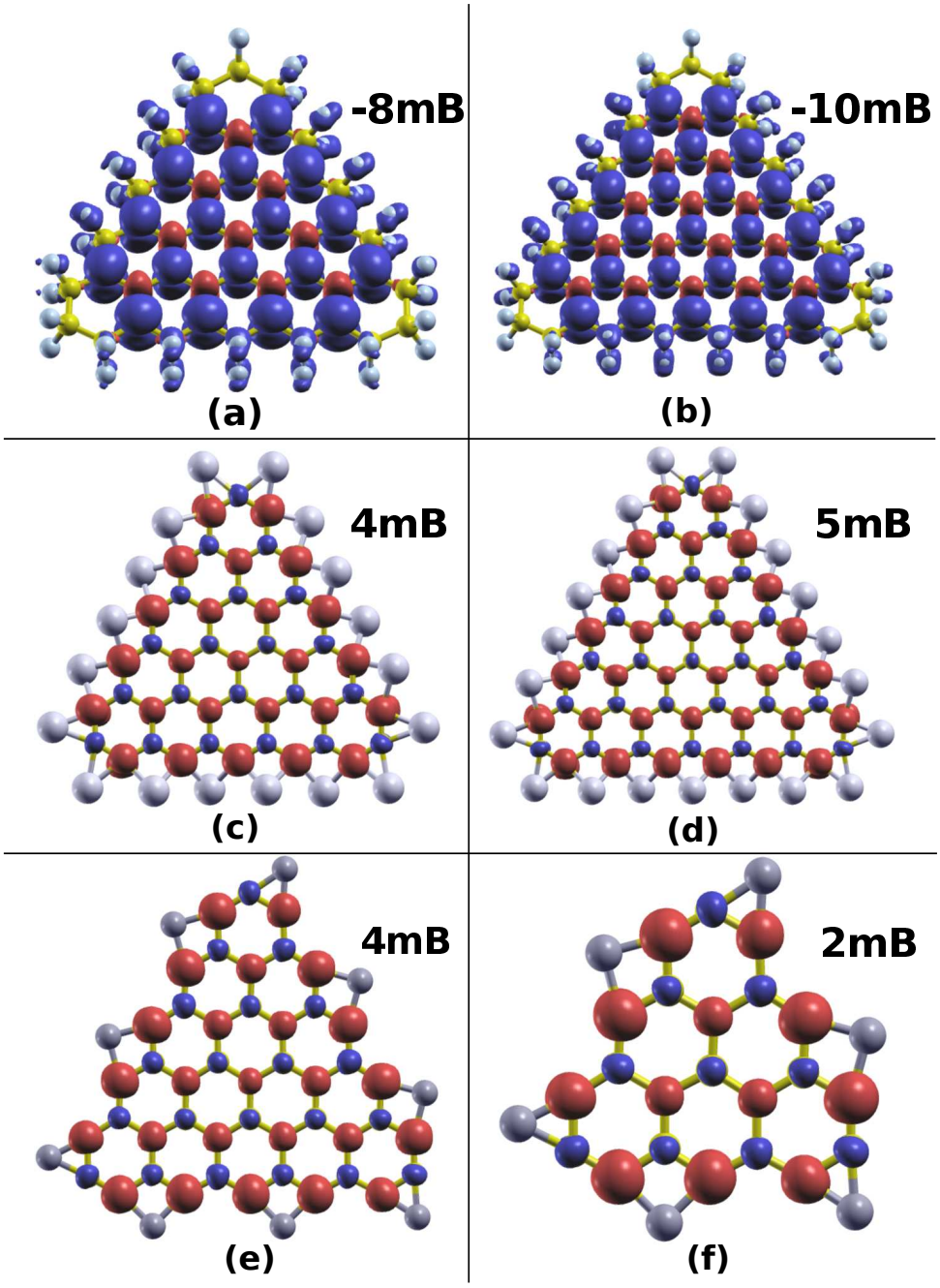

Figure 4.15. Isosurfaces of charge density difference of spin-up (↑) and spin-down (↓) states for all-edge-atoms-saturated TGFs; (a) 5-DC-F, (b) 6-DC-F, (c) 5-FC-Li, (d) 6-FC-Li, (e) 5-HC-Be, (f) 3-HC-Be.

magnetic of FC case become μ = (N-1), where N denotes the number of hexagons along each edge of TGF. As seen in Table 4.4, H atoms gain extra 25% of its valance charge from flake whereas F atoms charge transfer can be ignored.

On the other hand, in DC-H and DC-F cases, all the edge carbon atoms have sp^3 hybridized electrons with vanishing contribution to spin magnetic moment (see Table 4.4). Thus, in DC case, the net magnetic moment of TGF is given by $\mu = 2(N-1)\ \mu_B$, where the direction of magnetic moment is reversed. Table 4.4 shows that, in DC-H case, edge atoms of TGFs lose almost 10% of its valance charge while in DC-F charge transfer rather low.

In previous part that was found that, when single Be atom was added edge of TGF, the net magnetic moment of TGF reduce by 2. That result is deductive due to Be atom has two valence electron and these electrons eliminate two majority spin contribution of edge atoms. Thus, although adatom concentration of HC-Be is halve of FC-H and FC-F, the magnetic moment contribution of edge atoms same for all three cases and Figure 4.15 (e),(f) shows that, HC-Be cases magnetic moment is also given by $\mu = (N-1)\ \mu_B$.

Table 4.4. Calculated charge and magnetic moment values for all-edge-atoms-saturated 5-TGFs

	Total Charges			**Magnetic moments (μ_B)**		
	Edge C	**Adatoms**	**Bare Flake**	**Edge C**	**Adatoms**	**All Flake**
Bare flake	4.04	-	184.00	0.74	-	16
5-FC-H	3.77	1.26	179.38	0.20	0.00	4
5-DC-H	3.60	1.21	176.54	0.01	-0.03	-8
5-FC-F	4.09	6.90	185.85	0.17	0.02	4
5-DC-F	4.14	6.94	186.25	0.00	0.01	-8
5-FC-Li	4.20	0.84	186.82	0.18	0.00	4
5-HC-Be	4.06	1.99	184.10	0.18	-0.01	4

Up to now in this part, the net magnetic moment of HC-Be, FC-H, FC-F, DC-H and DC-F cases are invesitigated and either verifies the result of Lieb's Theorem or can be understood by simple modifications of it. However Li termination process utterly different. In the previous section it was mentioned that, although Li atom has only one valence charge, the net magnetic moment of TGF reduce by 3, when single Li atom is added edge of TGF. But, Figures 4.15 (c), (d) show that, FC-Li cases spin polarization distribution is the same with other FC structures.

To figure out the edge functionalization of TGFs by Li atoms, we removed one by one Li atoms from 5-FC-Li structure. Figure 4.16 shows the magnetic structures of Li removed cases from FC case to bare flake in order. As it is seen in Figure 4.16, there is not

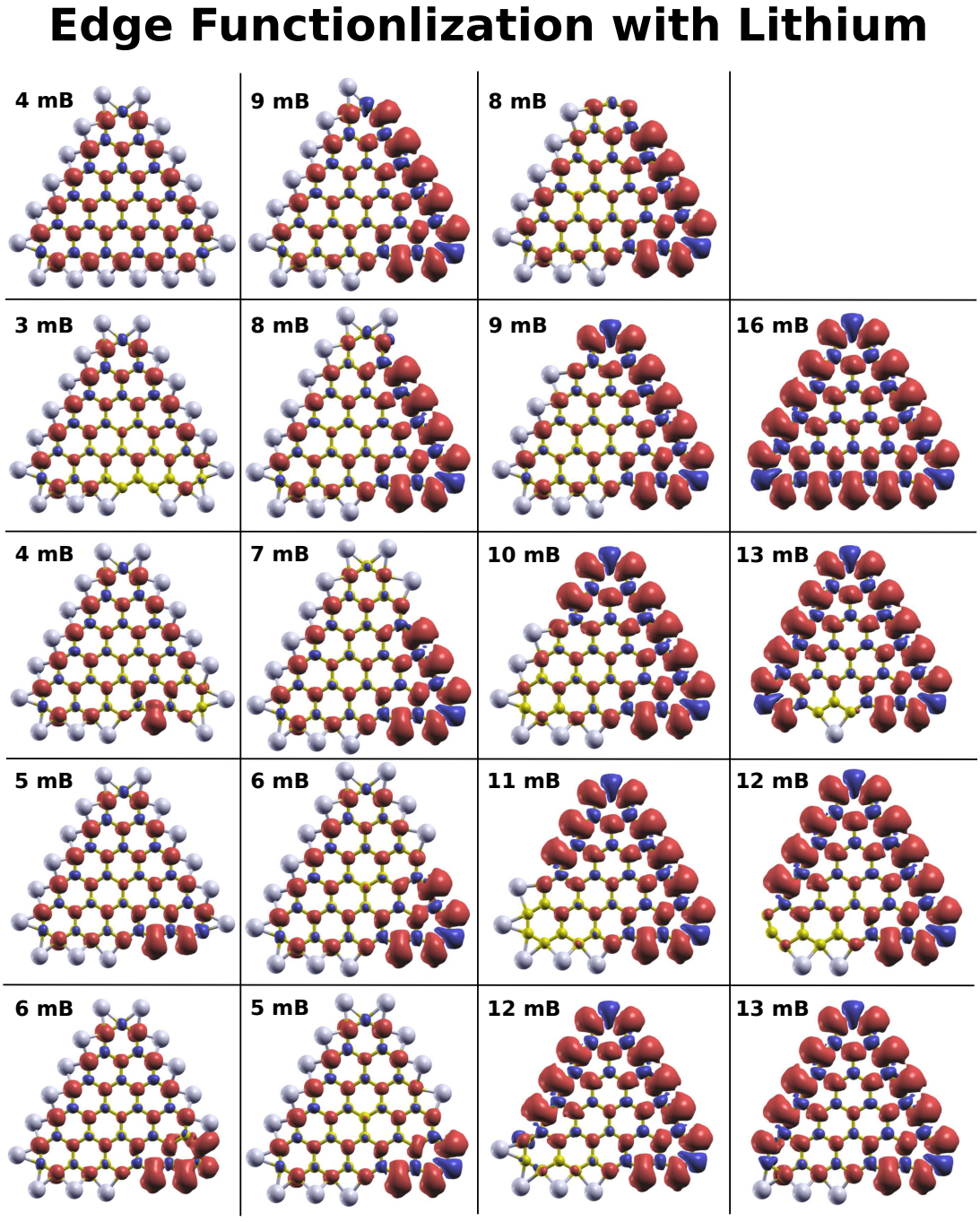

Figure 4.16. Isosurfaces of charge density difference of spin-up (↑) and spin-down (↓) states for Li removed cases from FC case to bare flake in order.

linear relation between adatom numbers and total magnetic moment of flake. When one Li atom was removed from FC-Li structure, total magnetic moment of flake decreased by one. If second Li atom was removed from TGF, the net magnetic moment of TGF raised by one due to one of the edge atoms having an extra nonbonding electron and in this situation TGF had the same net magnetic moment value with FC-Li case. After that, if we carry on to remove a Li atom one after another, the edge atom which Li atom was removed from it, became unsaturated in each time. If that unsaturated atom was an edge atom of TGF, the net magnetic moment of TGF increased by one. If that unsaturated atom was a corner atom of TGF, the net magnetic moment of TGF decreased by one. On the other hand when the last Li atom was removed from TGF, the total magnetic moment of TGF increased by three, and flake turns in to a bare TGF.

As a result, Figures 4.14, 4.15 and 4.16 shows that, the type of adatom does not change the spin localization structures. The concentration of adatoms significantly effect the spin localization structures of edge atoms. In FC case, contribution of the edge atoms to the magnetic moment was considerably low compared to bare flake, whereas in DC cases contribution of the edge atoms to the magnetic moment was vanishing. Furthermore it was found that magnetic moment of TGFs scale with its size. The magnetic properties of different covarage cases of TGF by H, F, Li, Be atoms, can be understood with Lieb's Theorem except two situations. The first one, when Li atom was removed from FC-Li structure, the magnetic moment of TGF was reduced by one while it was expected to be an increase. The second one, when last Li atom was removed from TGF, its magnetic moment increased by three, which it was expected to be increase by one. Table 4.4 shows that, when H atoms bind to TGF they got extra charge from flake, while other atoms lose their charge. In addition, Table 4.4 gives that there were no net induced magnetic moments on the H, F, Li and Be atoms in all cases.

CHAPTER 5

ELECTRIC-FIELD CONTROL OF MAGNETISM IN TGF

5.1. Introduction

In the previous chapter, we have considered edge functionalization of TGFs with various adatom types. We have found that electronic and magnetic properties of TGFs can be altered by size modifications, saturated with different adatom types and numbers. Experimentally these methods are quite difficult. However there is another way for manupulating of electric and magnetic properties of carbon nanostructures. Recent studies [71–73] have shown that the application of an electric field to graphene based nanostructures can alter their properties notably. The electrical manipulation of the magnetic properties of these nanostructures is quite important for the spintronic applications partly because it is easier to generate the electric field through local gate electrodes than the other methods such as chemical functionalization.

The aim of this chapter was to complete manipulation analysis of TGFs by considering the effect of electric field on these flakes. Earlier studies have shown that application of an electric field may be used for manipulation of the spin states in diamond-shaped graphene nanopatches [74], zigzag edged triangular graphene flakes [4] and bilayer zigzag edged triangular graphene flakes [3]. In fact, electric field effect on the properties of TGFs with density functional theory calculations has not yet been investigated. Motivated with these arguments, in this chapter, structural, electronic and magnetic properties of triangular graphene flakes are investigated under perpendicular and in-plane electric fields.

The electric field values were considered in this study in the order of volts per angstrom. Although such an electric field is large in a macrocopic scale, it is experimentally achievable for this nanostructures only if small electrodes can be made. In this chapter the first-principles density-functional calculations in the presence of an uniform electric field are performed using the SIESTA method. A periodic saw-tooth-type potential is used to simulate the external electric field in a supercell. Other components of the calculations are the same as those into previous chapter.

In this chapter we will study in detail the effect of an electric field on the geometric, electronic and magnetic structures of TGFs. Firstly we found that, large perpendicular electric field can make dramatic effects on the *geometric* structures of these flakes. How-

ever, our studies show that there is no significant effect of perpendicular electric field on the *electronic* and *magnetic* properties of these flakes. On the other hand, in-plane electric field significantly modifies all the properties of TGFs. For example large values of in-plane electric fields can remove corner atoms and make considerable distortions on the geometric structures of TGFs. Moreover, calculations have shown that HOMO-LUMO gaps of these TGFs may be tuned and total magnetic moments may be reduced by in-plane electric field.

5.2. Results

We will consider in-plane and perpendicular electric field effects. We show that external electric field can significantly change all the properties of TGFs and it is pretty usefull for manipulation of spin moment in TGFs.

5.2.1. Effects of In-Plane Electric Field on TGF

In this section, the external electric field, parallel to the *N*-TGF-H, is applied along X, Y and -Y directions. We found that in-plane electric field has notable effect on all the properties of TGFs. To investigate the effect of electric field we should examine Figure 5.1. The researcher assumes that *N*-TGF-H was placed into an external electric field of E and the size of *N*-TGF-H is d. Where E and d are in the units of V/Å and Å, respectively. The magnitude of the potential difference between the atoms, which are

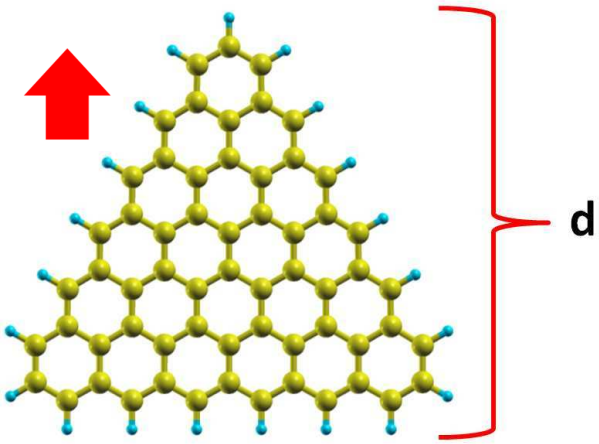

Figure 5.1. 6-TGF-H under the external electric field in the $+Y$-direction.

placed in two opposite sides of the flake, is $\Delta V = E * d$. Some edge and corner atoms will be exposured to large electric force, thus charge polarization occurs when an in-plane electric field applied. Moreover some corner atoms may break away from the *N*-TGF-H for large electric field values.

5.2.2. Geometric Structure

The geometric relaxation calculations under various values of electric field are done for different flake sizes *N*-TGF-H (*N* = 5, 6). Relaxed geometric structures and bond lenghts of 6-TGF-H for in the presence and absence of an electric field are shown in Figure 5.2.

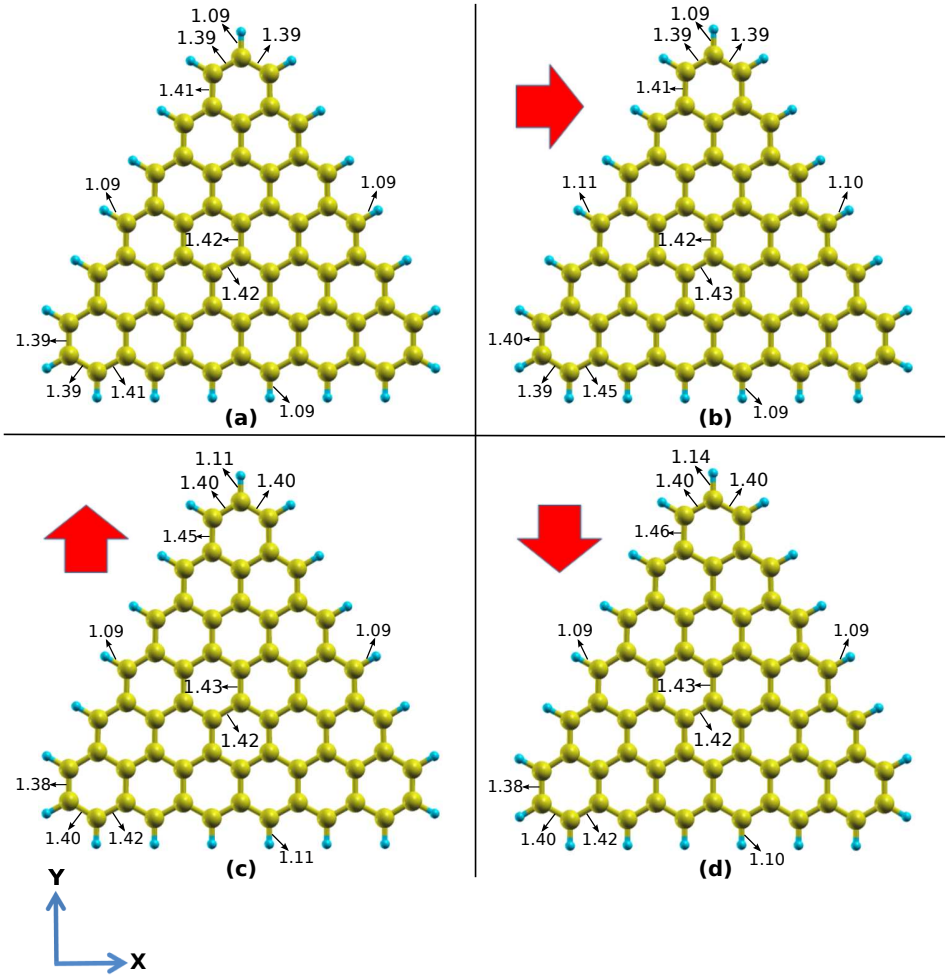

Figure 5.2. Relaxed geometric structures for 6-TGF-H under electric field with different directions: (a) 0 V/Å, (b) 1.4 V/Å in X direction, (c) 1.4 V/Å in Y direction, (d) -1.4 V/Å in Y direction (Red arrows representing the direction of electric field).

The change of geometric structure of 6-TGF-H in the electric field is similiar to the case of 5-TGF-H, so they are not given here. Figure 5.2 (a) shows the bond lenghts of 6-TGF-H under no electric field. Figure 5.2 (b)-(d) present the bond lenghts under in-plane electric field in the direction of X, Y, -Y, respectively, which applied electric field values are same for all the directions and their values are 1.4 V/Å. When greater electric field values are applied to the 6-TGF-H, geometric relaxations become difficult, flakes loose their geometric structures and some H atoms break away from the corner of 6-TGF-H. As can be seen from Figure 5.2, although flakes conserve their triangular geometries, bond lenghts between the atoms change with applied external electric field. The C-C bond lenghts which belong to the edge or corner atoms are more affected by applied electric field than those of center atoms of the flakes. The averaged C-C bond lenght is 1.4 Å near the corner of 6-TGF-H while it grows up to 1.46 Å under applied large electric field. The electrically induced failure is easier to occur at the corner of the 6-TGF-H since corner atoms are more susceptible relative to edge or center atoms of flake. Studies show that, when 6-TGF-H and 5-TGF-H are placed in the same electric field, 6-TGF-H has larger deformation than 5-TGF-H and the structure of 5-TGF-H is even stable under the electric field with value of 1.8 V/Å, which implies that small flakes are more stable than large flakes under the external in-plane electric field.

In the previous chapter it was mentioned that there is a relation between size and total magnetic moment of the flake as $\mu = (N-1)\,\mu_B$. Thus, odd sized flakes have an even magnetic moment values, whereas even sized flakes have an odd magnetic moment values. Using this fact, for a fixed total magnetic moment value of flakes we calculated total energy for various electric field values. Figure 5.3 presents the energies for different

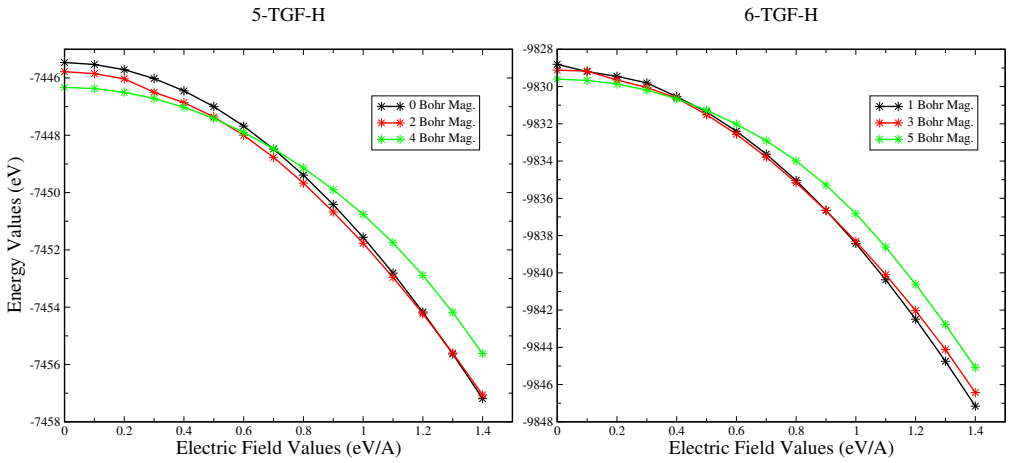

Figure 5.3. Energies of 5-TGF and 6-TGF with different total magnetic moment as a function of applied electric field.

magnetic moments of 5-TGF-H and 6-TGF-H as a function of an applied electric field. As it seen from Figure 5.3, there is a competiton among the energy values of different fixed magnetic moment values of flakes. Maximum spin polarized structure is favorable for both the absence of an electric field or applied small amount electric field. However, minimum spin polarized or non-spin polarized structures are favorable under large amount of applied electric field. Moreover, Figure 5.3 reveals that total energy of the flake decreases as both the size of the flake and the external applied electrical field increases.

The energies of different magnetic orders are investigated with respect to the ferromagnetic orders and shown in Figure 5.4. As it is seen from the figure there are some discontinuities in the energy values because of that flakes have maximum spin polarization in low electric field. Fixing the spin polarization at low values makes the calculations difficult and correct ground state energy values can not be obtained. In Figure 5.4, max-

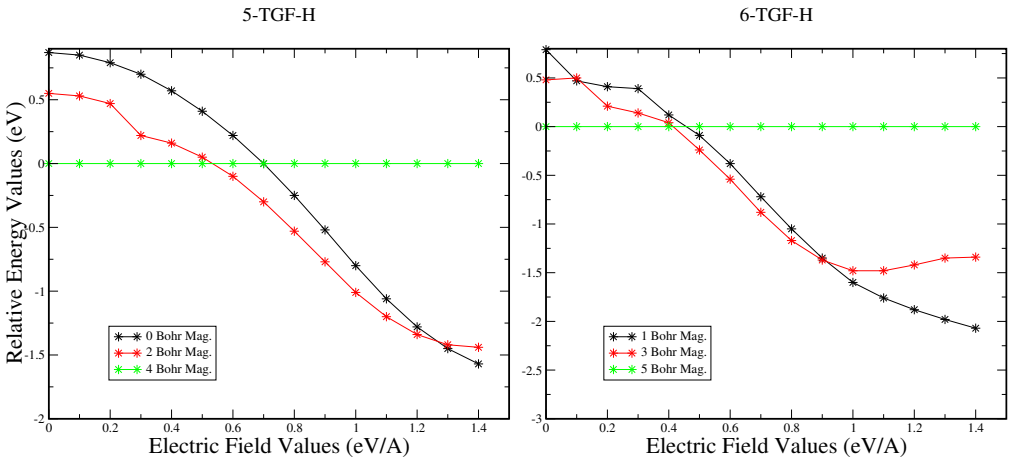

Figure 5.4. Energies of 5-TGF-H and 6-TGF-H with different total magnetic moment as a function of applied electric field, with respect to the configuration which have maximum magnetic moment.

imum spin polarized structure energies are shifted to 0 and the figure clearly shows that there are two critical electric field values for 5-TGF-H and 6-TGF-H seperately. In those critical electric field values, ground state total spin polarizations of flakes change and flakes prefer to have low spin polarization. These critical electric field values are 0.54 V/Å and 1.27 V/Å for 5-TGF-H and 0.41 V/Å and 0.91 V/Å for 6-TGF-H. These results reveal that when electric field is applied, the change in the ground state of total spin polarizations occurs in the larger flakes easier that in smaller flakes. If the electric field is increased more than the second critical electric field values, the total spin remains constant until the values of 1.4 V/Å and 1.8 V/Å for 6-TGF-H and 5-TGF-H, respectively. If the electric field is increased further, 5-TGF-H and 6-TGF-H loose their geometric structures

and some corner atoms break away from the flakes.

5.2.3. Electronic Structure

The electronic charge density distribution of the 6-TGF-H is shown in Figure 5.5 (a), in which the charge densities are shown by blue regions and isosurface value is 0.25 electrons/Å^3. As it is seen in the figure, the charges are localized between the C atoms and charge distribution is distributed smoothly all over the flake. Figures 5.5 (b)-(d) illustrate the change of the charge density distribution of 6-TGF-H with an external electric field along the X, Y and -Y directions, respectively. In these figures, applied electric field

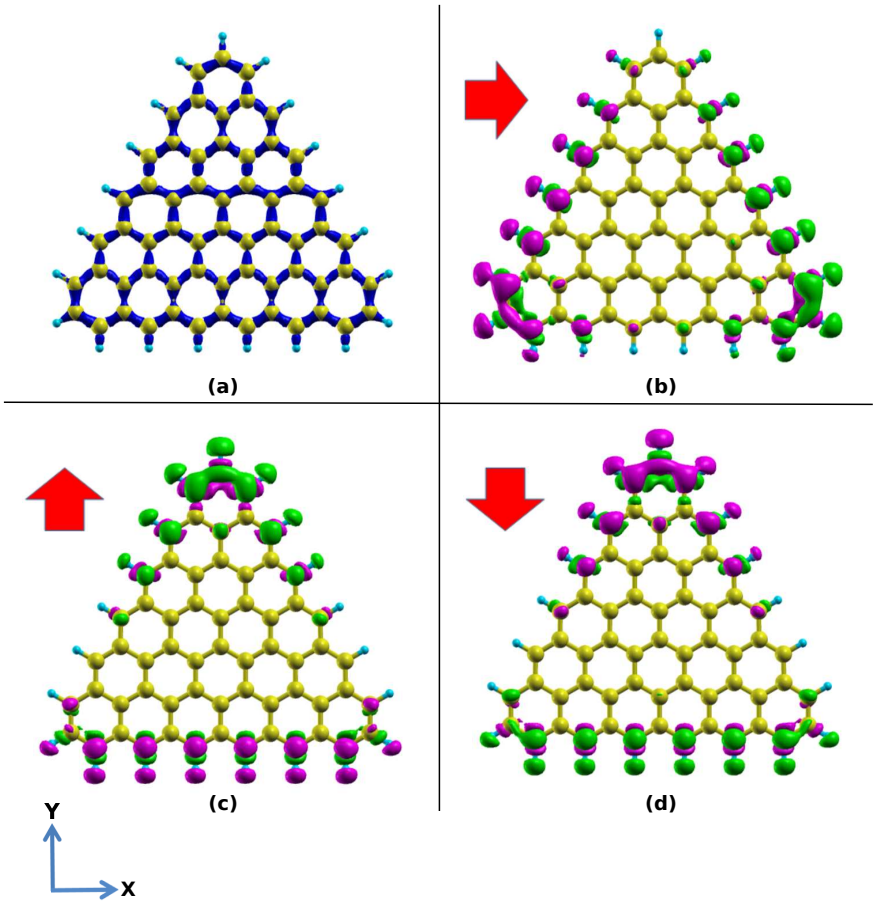

Figure 5.5. (a) Isosurfaces of charge density for 6-TGF-H in the absence of an electric field. The charge densities are shown by blue regions with isosurface value of 0.25 electrons/Å^3. (b)-(d) illustrate the change of the charge density distribution of 6-TGF-H with an external electric field along the X, Y and -Y directions, respectively. External electric field values are same and their values are 1.4 eV/Å. Purple regions denote increase, while green regions denote decrease in the charge densities for given regions.

values are the same and their magnitudes are 1.4 V/Å, purple regions denote an increase while the green ones denote a decrease in the charge density of the given regions. The application of an external electric field disrupt the symmetry of the charge density distribution. Since the electrons are known to move in opposite direction to an applied electric field, the charges of one side of flake decrease while the charges of the opposite side increase under applied in-plane electric field to 6-TGF-H in X-direction. On the other hand, when an electric field applied to 6-TGF-H in +Y-direction, the charges of the one side of the flake increase, the charges of the opposite corner of the flake decrease and vice versa for an applied electric field in -Y direction. This means that, under in-plane electric field 6-TGF-H is electrically polarized.

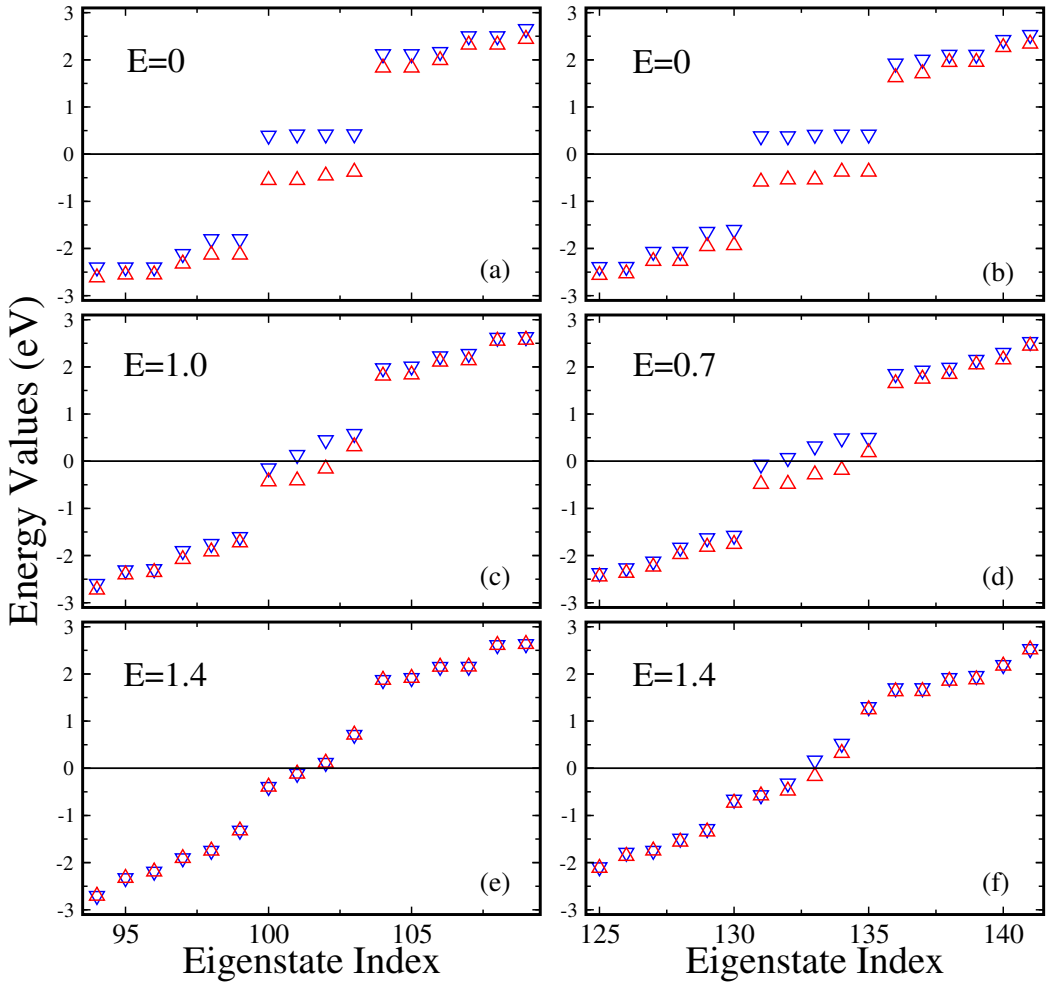

Figure 5.6. The energy spectra of 5-TGF-H (left) and 6-TGF-H (right) for different values of an electric field. The electric field values are in V/Å units. Blue triangles represent the minority spin while red triangles represent the majority spin. Fermi level shifted to 0.

We analyzed the electric field dependence of the energy spectra of 5-TGF-H and 6-TGF-H near the fermi level. Figures 5.6 (a) and (b) show the energy spectra near the fermi level in the absence of an electric field of 5-TGF-H and 6-TGF-H, respectively. In these figures, the valence states just below the fermi level are the majority of the spin component whereas the conduction states just above the fermi level, the minority. These uncoupled states belong to the edge C atoms of the *N*-TGF-H since the states of all the inner atoms are coupled. As seen in figures, both of the systems are maximally spin polarized if there is no external electric field. Figures 5.6 (c)-(f) show that application of an electric field lifts the non-degeneracy of the edge states and modifies significantly the energy spectra of these flakes. When the in-plane electric field is applied to these flakes the most energitic majority state will be empty and the lowest energitic minority state will be occupied. This means that as majority spin distribution of the edge C atoms decreases, the net magnetic moment of the flake decreases. As the electric field is increased further, the same process will continue until TGFs have a minimum magnetic moment which is 0 μ_B for odd N values and 1 μ_B for even N values.

The changes of the HOMO-LUMO gaps with respect to an external in-plane electric field are shown in Figure 5.7 for 5-TGF-H and 6-TGF-H. As seen from the figure, the application of an in-plane electric field to these flakes is effective in tuning the energy gap. The HOMO-LUMO gap values reduce significantly with an in-plane electric field and energy gaps have the smallest values around the critical electric field, which have been already given as 0.54 V/Å, 1.27 V/Å for 5-TGF-H and 0.41 V/Å, 0.91 V/Å for 6-TGF-H.

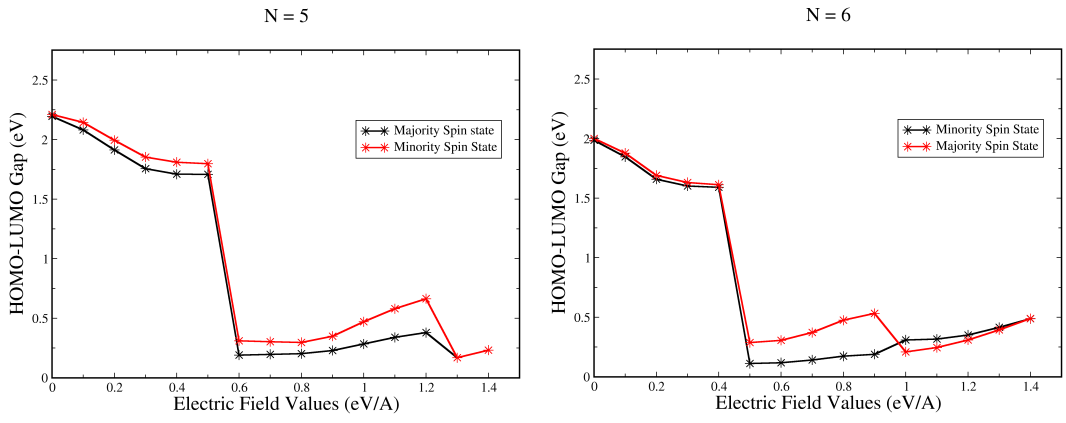

Figure 5.7. Change of HOMO-LUMO gap with respect to an applied electric field for 5-TGF-H and 6-TGF-H.

5.2.4. Magnetic Structure

The spin dependent charge density differences ($\triangle\ \rho = \rho_{\uparrow} - \rho_{\downarrow}$) of the optimized structures of 5-TGF-H are given in Figure 5.8. We have discussed in the previous chapter that in the absence of an electric field the total magnetic moment of 5-TGF-H is $4\ \mu_B$. However the application of an external electric field may have great influence on the spin-up, spin-down distributions of the 5-TGF-H displayed in Figure 5.8 (a)-(c). When in-plane electric field is applied to this flake, the total magnetic moment keeps constant until the electric field is beyond some critical value (0.54 V/Å), after which the total magnetic moment decreases to $2\ \mu_B$ (see figure 5.8(b)). If an in-plane electric field is applied to

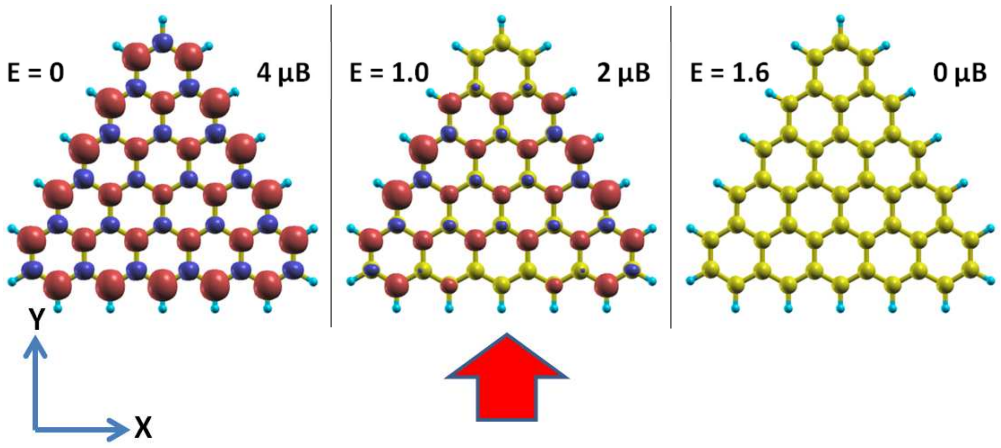

Figure 5.8. Isosurfaces of spin dependent charge density differeces for 5-TGF-H with and without the application of in-plane electric field. Electric field values are in V/Å units.

the flake, the electrons are forced to move in the opposite direction to the external electric field. Thus the spin-up and the spin-down densities on the edge and corner atoms of the flake, where the large charge transfer occured in, decrease almost the zero. As an electric field is increased further, the total magnetic moment remains constant until the electric field has some critical value beyond 1.27 V/Å, then the total magnetic moment decreases to $0\ \mu_B$ (see figure 5.8(c)), and all parts of the flake become non-magnetic.

Futhermore, the effect of direction of in-plane electric field on the spin dependent charge density distribution of *N*-TGF-H, have also been examined. The spin dependent charge density differences for 6-TGF-H in the absence of an electric field and under in-plane electric field along the X, Y, -Y directions are shown in Figures 5.9 (a)-(d), respectively. Applied electric field values are the same for the three figures (5.9 (b)-(d)), and their values are 1.4 V/Å. When these electric fields are applied to 6-TGF-H's, their

magnetic moments decrease to 1 μ_B. Apart from 5-TGF-H, it is not possible to have a completely vanishing of magnetic moment of 6-TGF-H. Applied electric field causes charge transfer along opposite of its direction. The spin polarizations vanish in the the place where the charge transfer is almost maximum. If electric field is applied along +X direction, this time spin polarization vanishes on the cornes of the edge that parallel to the applied electric field (Figure 5.9 (b)). If electric field is applied along $\pm$ Y direction, spin polarization vanishes on the edge that perpendicular to the applied electric field and the corner that on the opposite side of the edge (Figure 5.9 (c-d)). Thus, the distribution of spin-up and spin-down states is closely relevant to the direction of applied electric field.

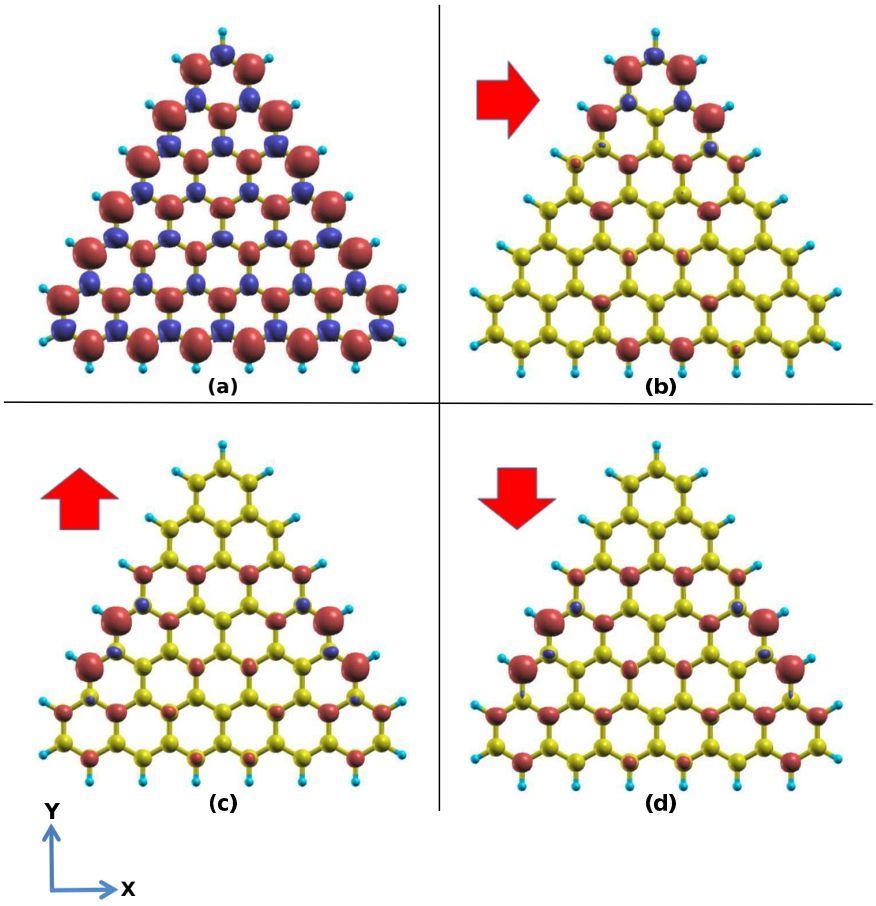

Figure 5.9. Isosurfaces of spin dependent charge density for 6-TGF-H with and without the application of in-plane electric field. Applied electric field values are same for (b)-(d) and their values are 1.4 V/Å.

Next we investigate the effect of an external electric field on the spin dependent charge density difference distribution, up spin states distribution and down spin states distribution, respectively. Figure 5.10 (a) displays the isosurface of the spin dependent charge density differences of 6-TGF-H. As seen in Figure 5.10 (b), when the electric field

is applied to flake, spin dependent charge density difference decreases significantly all over the part of the flake. Figures 5.10 (c) and (d) illustrate that when electric field applied to this flake, up-spin distribution decreases, while the down-spin distribution increases. From the figure it is seen that these decrease and increase in the up spin and down spin distributions mostly occur on the edge that perpendicular to the applied electric field and to the corner on the opposite side of this edge. Thus, up spin and down spin distributions are almost stationary on the two edges of TGF which are parallel to the applied in-plane electric field. In Figure 5.10, the purple regions denote an increase, while the green one denotes a decrease in the charge densities of the given regions and the applied electric field values are the same with the magnitude 1.4 V/Å.

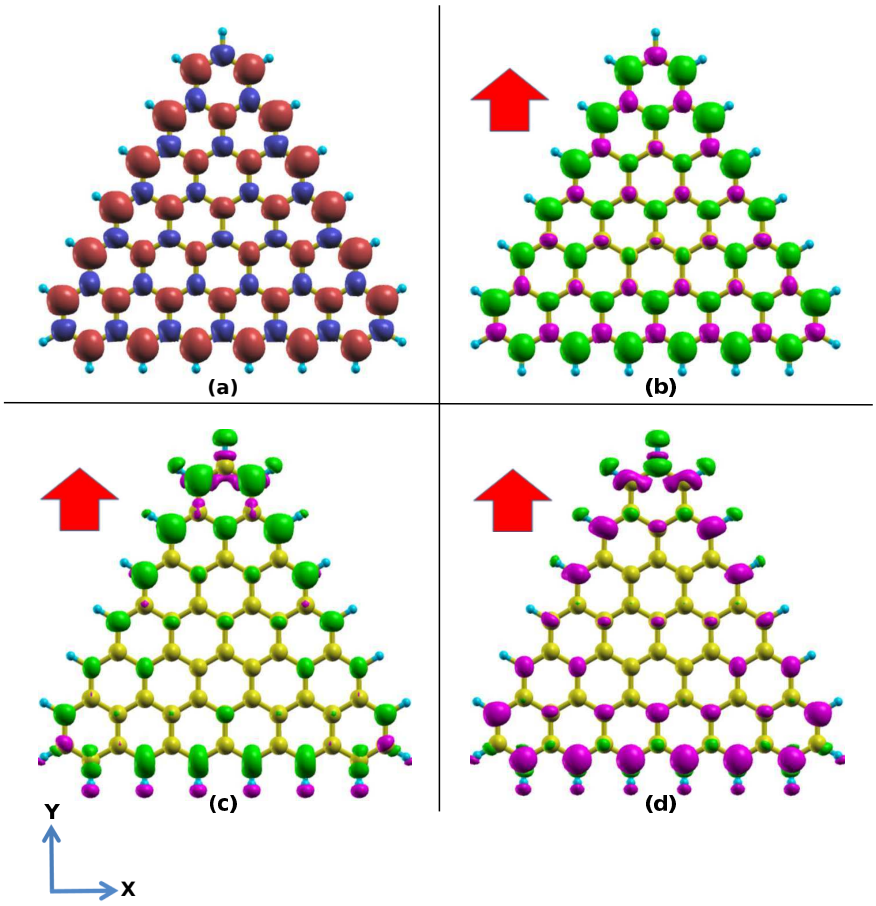

Figure 5.10. (a) Isosurfaces of the spin dependent charge density difference for 6-TGF-H. (b) Evolution in the the spin dependent charge density difference distribution, up-spin states distribution and down-spin states distribution with an applied electric field are shown in (b)-(d), respectively. While purple regions denotes increase, green regions denotes decrease in the charge densities for given regions. Applied electric field values are same for (b)-(d) and their values are 1.4 V/Å.

The variations in the total magnetic moment of 5-TGF-H and 6-TGF-H with respect to applied in-plane electric field are given in Figure 5.11. This figure shows that the total magnetic moment of the flakes reduces stepwise at the critical electric field values. Figure 5.11 shows the that total magnetic moments of the flake reduce by 2 bohr magneton when electric field is beyond some critical value. This means that one of the electrons

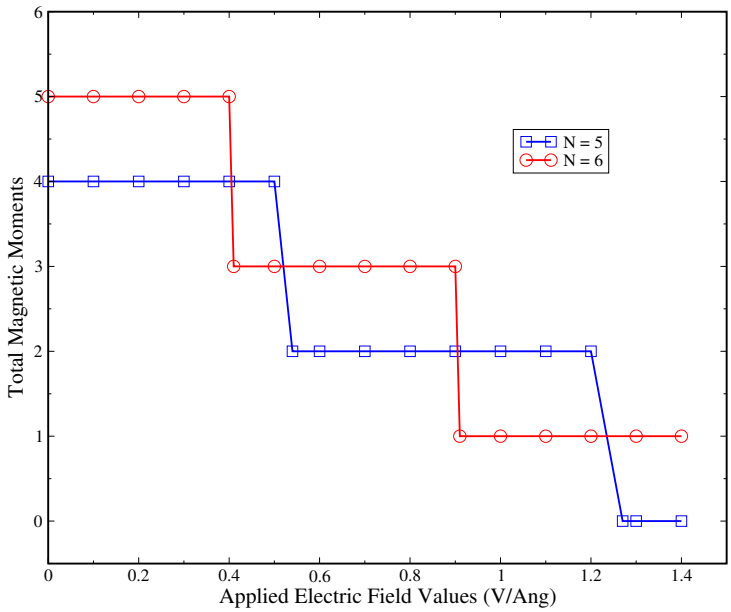

Figure 5.11. The total magnetic moment (in units of μ_B) of 5-TGF-H (blue line) and 6-TGF-H (red line) as a function of the electric field strenght (in units of V/Å).

of TGF which belongs to majority of the spin component, flips to minority spin component at the critical electric field. The total magnetic moments of the flake can minimally decrease to $0\ \mu_B$ for odd N values but complete spin depolarization cannot happen for even N values, since the number of electrons in the TGF is an odd number. Thus for even N values, the total magnetic moments of the flake can minimally be $1\ \mu_B$ with an applied electric field.

5.2.5. TGF Under a Perpendicular Electric Field

In this part, the effect of perpendicular electric field on the properties of hydrogenated TGFs is investigated. Relaxed geometric structures of 5-TGF-H in the absence of an electric field and in the presence of an electric field which directed perpendicular to the plane of 5-TGF-H, are both shown in Figure 5.12. Our calculations show that ge-

ometric, electric and magnetic structures of TGF remain the same for small electric field values. But as shown Figure 5.12, when electric field is increased, the geometric structure of 5-TGF-H is distorted and the planar geometry of the flake breaks down. The value of applied electric field is 2.1 V/Å for the given figure. For the values which are greater than this value of electric field, geometric relaxations become more difficult, flakes loose their geometric structures and some corner carbon and hydrogen atoms break away from the flake. The electrically induced failure is easier to occur at the corner of the flake.

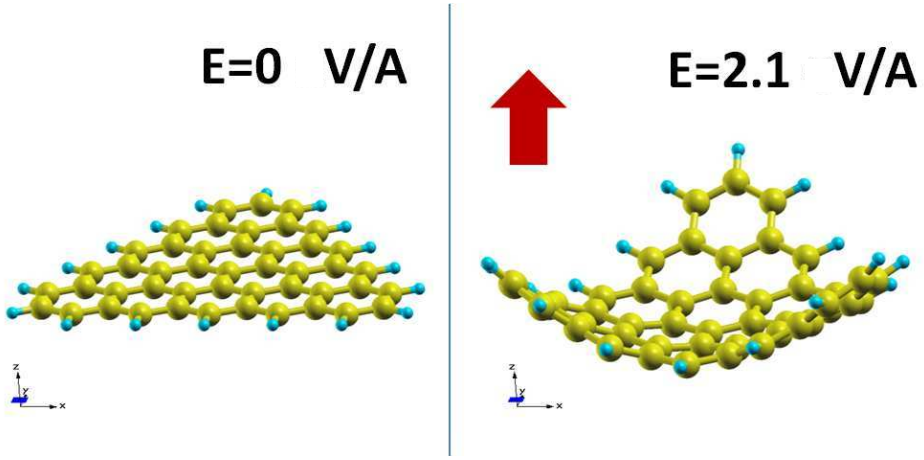

Figure 5.12. Relaxed geometric structures for 5-TGF-H: (a) In the absence of an electric field, (b) Under the perpendicular electric field.

As it is seen in Figure 5.12, perpendicular electric field makes significant distortions on the geometric structure of the 5-TGF-H. But, perpendicular electric field does not change the N_S value and the total magnetic moment of 5-TGF-H. Geometric distortions, which occur at perpendicular electric field applied to the TGFs, are interesting. This result indicate that by using the same procedure may be some suitable planar graphitic fragments can turn into fulleren structures under the perpendicular external electric field.

CHAPTER 6

CONCLUSIONS

Graphene based nano flakes are among the most promising materials for future nanoelectronics and spintronics. Edge localized spin polarizations of these flakes introduce magnetic properties that can be utilized for spintronic applications. To achive the purpose of using these flakes in electronic devices, magnetic moments of these flakes should be manipulated. Due to their special geometric structure, zigzag edged triangular graphene flakes (TGFs) have large magnetic moment and this magnetic moment can be manipulated by several means. With this motivation, the aim of this thesis was to study the electronic and magnetic properties of TGFs and to explore their manipulation. In this thesis two methods were considered for manipulation of electronic and magnetic properties of TGFs; which edge functionalization with adatoms and application of external electric field.

In the first case, several atoms (H, F, Li, Be, B, C and N) were used for saturating the dangling bonds of edge carbon atoms. The edge functionalization process is examined in two parts: First, we studied electronic and magnetic properties of bare and single-atom-added-TGFs. We found that, total magnetic moments of bare flakes are changing with $\mu = 4\,(N-1)\,\mu_B$, where *N* denotes the number of benzene rings on one edge of TGF. When a single atom bind to edge or corner of a TGF, total magnetic moment of the TGF changed. It was found that, total magnetic moment of the TGF strongly dependent on the binding site and the type of the adatom. While H, F, Li and Be atoms are nonmagnetic, B, C and N atoms showed magnetic behaviour when they bind to edge or corner of TGF and magnetic structures of all the cases can be explained with Lieb's theorem except for the single Li atom adding process. Although Li atom has one valence charge, when it binds to edge of TGF, it reduces magnetic moment of TGF by $3\ \mu_B$. Second, we studied saturation of all edge atoms of TGF. Three different concentrations of adatoms for saturation of edges are considered: 1) half-covarage (HC-X) where adatoms are bound to every other bridge site only, 2) full-covarage (FC-X) where there is one adatom for each edge atom, and 3) double-covarage (DC-X) where there are two adatoms for each edge atom. Here X denotes the type of the adatoms. FC-H, FC-F, FC-Li, DC-H, DC-F and HC-Be cases are examined. We found that, the total magnetic moment of FC-H, FC-F, FC-Li and HC-Be cases were $\mu = (N-1)\ \mu_B$. On the other hand the total magnetic moment of DC-H,

DC-F cases changed with $\mu = 2\ (N-1)\ \mu_B$ and the directions of total magnetic moment are reversed. Moreover, magnetic moments of all edge and corner atoms of TGF vanish in DC-H and DC-F cases. It was an intereseting found that although single Li saturation case did not obey Lieb's theorem, FC-Li case gave the same results with other FC cases and these results were in accordance with Lieb's theorem. Altogether, these results show that the net magnetic moment of TGF can be manipulated with edge or corner saturation processes.

In the second case, the effects of an external electric field on the electronic and magnetic properties of TGFs are investigated. It was found that geometric structures of TGFs were significantly changing with applied in-plane or perpendicular external electric fields. When perpendicular electric field applied total magnetic moment and number of spin non-degenerate states (N_S) of TGF did not change. But perpendicular electric field causes considerable distortions on the geometric structure of TGF and it distorts planar structure of TGF. Then we applied in-plane electric field in the X, Y and $-Y$ directions and observed how electronic and magnetic properties of TGFs changed. When in-plane electric field was applied to TGF, it polarizes the charge distribution in the flake. We saw that in the energy spectra, when the in-plane electric field applied to TGFs, the most energetic majority state will be empty and the lowest energetic minority state will be occupied. This means that, in these flakes total spin polarization can be reduced stepwise with the applied in-plane electric field. If a sufficient electric field is applied to odd-sized TGF all the polarized spins disappear. However, completely vanishing of polarized spin states of TGFs is not possible for even sized flakes. These results opens a way to electrically manupilating magnetic moments of small graphene flakes.

REFERENCES

[1] Motohiko Ezawa. Metallic graphene nanodisks: Electronic and magnetic properties. *Physical Review B*, 76(24):245415, 2007.

[2] H Şahin and Ramazan Tugrul Senger. First-principles calculations of spin-dependent conductance of graphene flakes. *Physical Review B*, 78(20):205423, 2008.

[3] A. D. Güçlü, P. Potasz, and P. Hawrylak. Electric-field controlled spin in bilayer triangular graphene quantum dots. *Phys. Rev. B*, 84:035425, Jul 2011.

[4] Wen-Long Ma and Shu-Shen Li. Electric-field-induced spin depolarization in graphene quantum dots. *Phys. Rev. B*, 86:045449, Jul 2012.

[5] M. N. Baibich, J. M. Broto, A. Fert, F. Nguyen Van Dau, F. Petroff, P. Etienne, G. Creuzet, A. Friederich, and J. Chazelas. Giant magnetoresistance of (001)fe/(001)cr magnetic superlattices. *Phys. Rev. Lett.*, 61:2472–2475, Nov 1988.

[6] JMD Coey, M Venkatesan, CB Fitzgerald, AP Douvalis, and IS Sanders. Ferromagnetism of a graphite nodule from the canyon diablo meteorite. *Nature*, 420(6912):156–159, 2002.

[7] Tatiana L Makarova, Bertil Sundqvist, Roland Höhne, Pablo Esquinazi, Yakov Kopelevich, Peter Scharff, Valerii A Davydov, Ludmila S Kashevarova, and Aleksandra V Rakhmanina. Magnetic carbon. *Nature*, 413(6857):716–718, 2001.

[8] Juan M Manriquez, Gordon T Yee, R Scott McLean, ARTHUR J EPSTEIN, and JOEL S MILLER. A room-temperature molecular/organic-based magnet. *Science*, 252(5011):1415–1417, 1991.

[9] P. O. Lehtinen, A. S. Foster, A. Ayuela, A. Krasheninnikov, K. Nordlund, and R. M. Nieminen. Magnetic properties and diffusion of adatoms on a graphene sheet. *Phys. Rev. Lett.*, 91:017202, Jun 2003.

[10] P. O. Lehtinen, A. S. Foster, A. Ayuela, T. T. Vehviläinen, and R. M. Nieminen. Structure and magnetic properties of adatoms on carbon nanotubes. *Phys. Rev. B*, 69:155422, Apr 2004.

[11] Yoshiyuki Shibayama, Hirohiko Sato, Toshiaki Enoki, and Morinobu Endo. Disordered magnetism at the metal-insulator threshold in nano-graphite-based carbon materials. *Phys. Rev. Lett.*, 84:1744–1747, Feb 2000.

[12] Alexandre R Rocha, Victor M Garcia-Suarez, Steve W Bailey, Colin J Lambert, Jaime Ferrer, and Stefano Sanvito. Towards molecular spintronics. *Nature Materials*, 4(4):335–339, 2005.

[13] KS Novoselov, Andre K Geim, SV Morozov, D Jiang, Y Zhang, SV Dubonos, IV Grigorieva, and AA Firsov. Electric field effect in atomically thin carbon films. *Science*, 306(5696):666–669, 2004.

[14] KI Bolotin, KJ Sikes, J Hone, HL Stormer, and P Kim. Temperature-dependent transport in suspended graphene. *Physical review letters*, 101(9):096802, 2008.

[15] KS Novoselov, Ak K Geim, SV Morozov, D Jiang, MI Katsnelson IV Grigorieva, SV Dubonos, and AA Firsov. Two-dimensional gas of massless dirac fermions in graphene. *nature*, 438(7065):197–200, 2005.

[16] Konstantin S Novoselov, Z Jiang, Y Zhang, SV Morozov, HL Stormer, U Zeitler, JC Maan, GS Boebinger, P Kim, and AK Geim. Room-temperature quantum hall effect in graphene. *Science*, 315(5817):1379–1379, 2007.

[17] Changgu Lee, Xiaoding Wei, Jeffrey W Kysar, and James Hone. Measurement of the elastic properties and intrinsic strength of monolayer graphene. *science*, 321(5887):385–388, 2008.

[18] Jae Hun Seol, Insun Jo, Arden L Moore, Lucas Lindsay, Zachary H Aitken, Michael T Pettes, Xuesong Li, Zhen Yao, Rui Huang, David Broido, et al. Two-dimensional phonon transport in supported graphene. *Science*, 328(5975):213–216, 2010.

[19] Daniel Huertas-Hernando, F. Guinea, and Arne Brataas. Spin-orbit coupling in curved graphene, fullerenes, nanotubes, and nanotube caps. *Phys. Rev. B*, 74:155426, Oct 2006.

[20] Daniel Huertas-Hernando, Francisco Guinea, and Arne Brataas. Spin relaxation times in disordered graphene. *The European Physical Journal Special Topics*, 148(1):177–181, 2007.

[21] Andrey Chuvilin, Jannik C Meyer, Gerardo Algara-Siller, and Ute Kaiser. From

graphene constrictions to single carbon chains. *New Journal of Physics*, 11(8):083019, 2009.

[22] Chuanhong Jin, Haiping Lan, Lianmao Peng, Kazu Suenaga, and Sumio Iijima. Deriving carbon atomic chains from graphene. *Phys. Rev. Lett.*, 102:205501, May 2009.

[23] Young-Woo Son, Marvin L. Cohen, and Steven G. Louie. Energy gaps in graphene nanoribbons. *Phys. Rev. Lett.*, 97:216803, Nov 2006.

[24] Oleg V. Yazyev and M. I. Katsnelson. Magnetic correlations at graphene edges: Basis for novel spintronics devices. *Phys. Rev. Lett.*, 100:047209, Jan 2008.

[25] J Akola, HP Heiskanen, and M Manninen. Edge-dependent selection rules in magic triangular graphene flakes. *Physical Review B*, 77(19):193410, 2008.

[26] P Potasz, AD Güçlü, O Voznyy, JA Folk, and P Hawrylak. Electronic and magnetic properties of triangular graphene quantum rings. *Physical Review B*, 83(17):174441, 2011.

[27] Wei L Wang, Sheng Meng, and Efthimios Kaxiras. Graphene nanoflakes with large spin. *Nano letters*, 8(1):241–245, 2008.

[28] Hasan Sahin, R Tugrul Senger, and Salim Ciraci. Spintronic properties of zigzag-edged triangular graphene flakes. *Journal of Applied Physics*, 108(7):074301–074301, 2010.

[29] Elliott H Lieb. Two theorems on the hubbard model. *Physical review letters*, 62(10):1201–1204, 1989.

[30] P. Esquinazi, A. Setzer, R. Höhne, C. Semmelhack, Y. Kopelevich, D. Spemann, T. Butz, B. Kohlstrunk, and M. Lösche. Ferromagnetism in oriented graphite samples. *Phys. Rev. B*, 66:024429, Jul 2002.

[31] Tatiana Makarova and Fernando Palacio. *Carbon based magnetism: an overview of the magnetism of metal free carbon-based compounds and materials*, volume 10. Elsevier Science, 2006.

[32] RA Wood, MH Lewis, MR Lees, SM Bennington, MG Cain, and N Kitamura. Ferromagnetic fullerene. *Journal of Physics: Condensed Matter*, 14(22):L385, 2002.

[33] Andre K Geim and Konstantin S Novoselov. The rise of graphene. *Nature materials*, 6(3):183–191, 2007.

[34] PR Wallace. The band theory of graphite. *Physical Review*, 71(9):622, 1947.

[35] AH Castro Neto, F Guinea, NMR Peres, KS Novoselov, and AK Geim. The electronic properties of graphene. *Reviews of modern physics*, 81(1):109, 2009.

[36] Hosik Lee, Young-Woo Son, Noejung Park, Seungwu Han, and Jaejun Yu. Magnetic ordering at the edges of graphitic fragments: Magnetic tail interactions between the edge-localized states. *Physical Review B*, 72(17):174431, 2005.

[37] JJ Palacios, Joaquín Fernández-Rossier, and L Brey. Vacancy-induced magnetism in graphene and graphene ribbons. *Physical Review B*, 77(19):195428, 2008.

[38] Oleg V Yazyev and Lothar Helm. Defect-induced magnetism in graphene. *Physical Review B*, 75(12):125408, 2007.

[39] Sergey Mikhailov. *Physics and Applications of Graphene: Theory*. InTech, 2011.

[40] Melinda Y Han, Barbaros Özyilmaz, Yuanbo Zhang, and Philip Kim. Energy band-gap engineering of graphene nanoribbons. *Physical review letters*, 98(20):206805, 2007.

[41] Xiaolin Li, Xinran Wang, Li Zhang, Sangwon Lee, and Hongjie Dai. Chemically derived, ultrasmooth graphene nanoribbon semiconductors. *Science*, 319(5867):1229–1232, 2008.

[42] Alessandro Cresti, Giuseppe Grosso, and Giuseppe Pastori Parravicini. Numerical study of electronic transport in gated graphene ribbons. *Phys. Rev. B*, 76:205433, Nov 2007.

[43] Motohiko Ezawa. Peculiar width dependence of the electronic properties of carbon nanoribbons. *Phys. Rev. B*, 73:045432, Jan 2006.

[44] Oded Hod, Verónica Barone, Juan E Peralta, and Gustavo E Scuseria. Enhanced half-metallicity in edge-oxidized zigzag graphene nanoribbons. *Nano letters*, 7(8):2295–2299, 2007.

[45] Sujit S Datta, Douglas R Strachan, Samuel M Khamis, and AT Charlie Johnson. Crys-

tallographic etching of few-layer graphene. *Nano letters*, 8(7):1912–1915, 2008.

[46] Levente Tapasztó, Gergely Dobrik, Philippe Lambin, and Laszlo P Biro. Tailoring the atomic structure of graphene nanoribbons by scanning tunnelling microscope lithography. *Nature nanotechnology*, 3(7):397–401, 2008.

[47] F Chen and NJ Tao. Electron transport in single molecules: from benzene to graphene. *Accounts of chemical research*, 42(3):429–438, 2009.

[48] M. C. Payne, M. P. Teter, D. C. Allan, T. A. Arias, and J. D. Joannopoulos. Iterative minimization techniques for *ab initio* total-energy calculations: molecular dynamics and conjugate gradients. *Rev. Mod. Phys.*, 64:1045–1097, Oct 1992.

[49] Douglas R Hartree. The wave mechanics of an atom with a non-coulomb central field. part i. theory and methods. In *Mathematical Proceedings of the Cambridge Philosophical Society*, volume 24, pages 89–110. Cambridge Univ Press, 1928.

[50] J. C. Slater. The theory of complex spectra. *Phys. Rev.*, 34:1293–1322, Nov 1929.

[51] V Fock. Z. physik 61, 126 (1930); jc slater. *Phys. Rev*, 35:210, 1930.

[52] Paul AM Dirac. Note on exchange phenomena in the thomas atom. In *Proceedings of the Cambridge Philosophical Society*, volume 26, page 376, 1930.

[53] P. Hohenberg and W. Kohn. Inhomogeneous electron gas. *Phys. Rev.*, 136:B864–B871, Nov 1964.

[54] W. Kohn and L. J. Sham. Self-consistent equations including exchange and correlation effects. *Phys. Rev.*, 140:A1133–A1138, Nov 1965.

[55] R. P. Feynman. Forces in molecules. *Phys. Rev.*, 56:340–343, Aug 1939.

[56] Hans Hellmann. *Einführung in die quantenchemie: Texte imprimé*. F. Deuticke, 1937.

[57] O. H. Nielsen and Richard M. Martin. Quantum-mechanical theory of stress and force. *Phys. Rev. B*, 32:3780–3791, Sep 1985.

[58] O. H. Nielsen and Richard M. Martin. Stresses in semiconductors: *Ab initio* calculations on si, ge, and gaas. *Phys. Rev. B*, 32:3792–3805, Sep 1985.

[59] D. M. Ceperley and B. J. Alder. Ground state of the electron gas by a stochastic method.

Phys. Rev. Lett., 45:566–569, Aug 1980.

[60] J. Fernández-Rossier and J. J. Palacios. Magnetism in graphene nanoislands. *Phys. Rev. Lett.*, 99:177204, Oct 2007.

[61] Oded Hod, Juan E Peralta, and Gustavo E Scuseria. Edge effects in finite elongated graphene nanoribbons. *Physical Review B*, 76(23):233401, 2007.

[62] Mohammad Zarenia, Andrey Chaves, GA Farias, and FM Peeters. Energy levels of triangular and hexagonal graphene quantum dots: A comparative study between the tight-binding and dirac equation approach. *Physical Review B*, 84(24):245403, 2011.

[63] A. V. Rozhkov and Franco Nori. Exact wave functions for an electron on a graphene triangular quantum dot. *Phys. Rev. B*, 81:155401, Apr 2010.

[64] Björn Trauzettel, Denis V Bulaev, Daniel Loss, and Guido Burkard. Spin qubits in graphene quantum dots. *Nature Physics*, 3(3):192–196, 2007.

[65] Oleg V Yazyev. Emergence of magnetism in graphene materials and nanostructures. *Reports on Progress in Physics*, 73(5):056501, 2010.

[66] Xiaoting Jia, Mario Hofmann, Vincent Meunier, Bobby G Sumpter, Jessica Campos-Delgado, José Manuel Romo-Herrera, Hyungbin Son, Ya-Ping Hsieh, Alfonso Reina, Jing Kong, et al. Controlled formation of sharp zigzag and armchair edges in graphitic nanoribbons. *Science*, 323(5922):1701–1705, 2009.

[67] Chee Kwan Gan and David J. Srolovitz. First-principles study of graphene edge properties and flake shapes. *Phys. Rev. B*, 81:125445, Mar 2010.

[68] W Sheng, ZY Ning, ZQ Yang, and H Guo. Magnetism and perfect spin filtering effect in graphene nanoflakes. *Nanotechnology*, 21(38):385201, 2010.

[69] Wei Zhang, Litao Sun, Zijian Xu, Arkady V. Krasheninnikov, Ping Huai, Zhiyuan Zhu, and F. Banhart. Migration of gold atoms in graphene ribbons: Role of the edges. *Phys. Rev. B*, 81:125425, Mar 2010.

[70] Motohiko Ezawa. Graphene nanoribbon and graphene nanodisk. *Physica E: Low-dimensional Systems and Nanostructures*, 40(5):1421–1423, 2008.

[71] Jun Hu and Ruqian Wu. Control of the magnetism and magnetic anisotropy of a single-molecule magnet with an electric field. *Phys. Rev. Lett.*, 110:097202, Feb 2013.

[72] Taisuke Ohta, Aaron Bostwick, Thomas Seyller, Karsten Horn, and Eli Rotenberg. Controlling the electronic structure of bilayer graphene. *Science*, 313(5789):951–954, 2006.

[73] Young-Woo Son, Marvin L Cohen, and Steven G Louie. Half-metallic graphene nanoribbons. *Nature*, 444(7117):347–349, 2006.

[74] Luis A Agapito, Nicholas Kioussis, and Efthimios Kaxiras. Electric-field control of magnetism in graphene quantum dots: Ab initio calculations. *Physical Review B*, 82(20):201411, 2010.